TR/05/92 JUNE 1992

The 3D Version of the Finite Element Program FESTER

—A Technical Report

Ruibn Qu and Martin B. Reed

The 3D Version of the Finite Element Program FESTER —A Technical Report

Ruibin Qu and Martin B. Reed
Department of Mathematics and Statistics,
Brunel University, Uxbridge, Middx.., UB8 3PH, Britain
April 1991

Abstract

In this report, a detailed description of the 3-D version finite element program **FESTER** *is given. This includes:* **1**. *A brief introduction to the package* **FESTER**; **2**. *Preparing an input data file for the 3D version of* **FESTER;** **3**. *Principal stress and stress invariant analyses;* **4.** *2D joint element (surface contact) characterisation and its mathematical formulation;* **5.** *Formulations of the* **3D** *stress-strain analyses for both isotropic and anisotropic materials, plane of weakness and cracking criteria;* **6.** ***3D*** *brick elements, infinity elements and their corresponding shape and mapping functions;* **7.** *Large-displacement formulations;* **8.** *Modifications to the subroutines* **INVAR, JNTB, TMAT, MOD2** *etc;* **9.** *Numerical examples; and* **10.** *Conclusions.*

§1. An introduction to FESTER

In this section, we present a brief introduction to the finite element package **FESTER** (Finite Element Simulation of Tunnelling & Excavation in Rocks).

1.1. Development of FESTER

The computer program **FESTER** was originally developed on an **SERC**/British Coal co-funded research project at the Oxford University Computing Laboratory between 1985 and 1986. Since the end of 1986, it has been continuously developed at the Department of Mathematics and Statistics of Brunel University under the support of **SERC** (current grant is to finish in 1992) and British Coal (finished in 1988). The program structure is based on the linear elastic finite element package **FINEPACK** developed at the Department of Civil Engineering of University College Swansea [13,20,21,etc.] **FESTER** is developed to model the deformation and stresses in the rock mass surrounding

underground openings and to predict the failure behaviour of rock masses. It uses elasto-viscoplastic theory for the nonlinear analysis. The detailed theory and features including a user's guide can be found in a previous report [32]. Some of the work involved in the development of the program was also reported in several published papers by the main developer Reed [30-34]. Since 1989, the program has been further developed to incorporate a few other features based on the co-operative research work at the Rock Mechanics Research Group of Imperial College [22-27].

Since July 1990, **FESTER** has been developed to cope with 3-D stress-strain analyses for both isotropic and anisotropic rocks. It is mainly aimed at analysing deep-level excavations using 3-D finite elements, including infinite elements and joint elements (2D contact). This work includes the introduction of 8-noded and 20-Noded brick elements, an infinite element, 2-D joint element, 3-D rock mass strata modelling, the numerical algorithm for 3-D stress-strain analyses for elasto-viscoplastic rock models etc.

1.2. Mathematical models in 3-D FESTER

The 3-D version of the program **FESTER** is an (3-D) elasto-viscoplastic finite element model for analysis of rock and rock mass behaviour. It is developed from its previous 2-D version which is described in detail in [20,27,32,34]. The theory and numerical algorithm are almost the same but the formulations may be different. The main features of the analyses, in addition to that described in [34], are as follows:

A. 3D Element types:

The following types of element are used in **FESTER:**

(i). the 8-noded linear brick element for representing the rock mass;

(ii). the isoparametric 20-noded quadratic brick element for representing the rock mass;

(iii). the 12-noded mapped infinite element for representing far field boundary, and

(iv). the 16-noded joint element for discontinuities in displacements and shear strains.

B. Nonlinear techniques:

Incremental (tangent stiffness) approach with the stable implicit ($\frac{1}{2} < \theta \leq 1$) or explicit ($\theta = 0$) time integration algorithm. Use of a non-symmetric frontal method. Options for large deformation analysis with Updated Lagrangian formulation.

C. Rock mass models:

Orthotropic elasticity; elastic joint interface (2-D); brittle/strain softening failure or yield with Mohr-Coulomb, Drucker-Prager or Hoek-Brown 3-D surface; asso-

ciated/nonassociated flow rule with Drucker-Prager or the extended Hoek-Brown flow function. Options for two other failure modes: tensile crack and fracture along the plane of weakness in the orthotropic case.

D. Types of loading:

Point loads; edge loads, distributed surface loads (restricted to Normal Loads only), body forces; gravity and other *in situ* stress fields; incremental loading; two ways of simulating excavation (opposite nodal forces or reduction of stress and stiffness) which can be combined without any restriction.

E. Boundary conditions:

Infinite elements to model far field boundary conditions; prescribed values of displacement or pressure at the boundary element nodes, edges or surfaces.

F. Sliding between two rock strata

2D joint elements to tackle the problems of discontinuous displacements, stresses and strains between two rock strata, and in the plane of weakness for orthotropic rock masses.

§2. Input data file formats and variable names

The 3-D version of the program **FESTER** is based on its 2-D version and hence it can also be used to solve 2-D and axisymmetric problems. The structure of the input data file is the same as in the 2-D case which is described in Reed and Lavender [34] and Naylor [20]. In this section, we give the detailed order and formats of the input data file since the file can be prepared by hand, in case that a 3-D preprocessor for **FESTER** is not available. In the following descriptions of the formats and the variables to be read, the order and their names in parenthesis, *i.e.,* G2, B1 and P2 etc., of the "Data Cards" are also listed. It should be pointed out that the variable LCARD in the following list is a "flag" which is used to terminate a read loop (*i. e.,* to terminate a data subset) when its value is 1. Otherwise, it should be set to 0 or left blank. An example input file will be given in §9.

2.1. Input data file formats

In an input file, there are at most twenty Data subsets which are to be read into **FESTER** described by twenty Read format Statements. There may be fewer, depending

on loading processes, boundary conditions and default values etc. for the particular problem to be analysed. The formats and variables to be input to **FESTER** are listed in the following table.

A typical input data file			
No.	Type	Input Format	Variables Read
1	TITLE	[I1,A50]	IPOST,TITLE
2	C1	[12I5]	NPOIN,NELEM,NFIXV,MSTYP,NDIME,
			NODEM,NDOFM,NGAUS,NSTRE,NLAPS,
			NEXCA,NCALL
3	C2	[12I5]	NPROS,NPROP,NOUT,NBDRY,NGRIS,
			LDTYP,NINCS,NITER,NBSET,NPSET,
			spare,spare
4	C3	[8E10.3]	TOLER,DTINT,TAUFT,FTIME,YDMIN,
			ALLOW,TIMEX,FLOWC
5	G1	[11,14,13I5]	LCARD,NSIDE,LNUM,LNODS(LNUM,I),
			(I=1,NNODE)
6	G2	[11,14,15,3E10.3]	LCARD,NDOFN,N,COORD(N,I),
			(I=1,3)
7	G3	[11,19,1415]	LCARD,KODE,NO.-of-Node
8	LM	[11,I4,15I5]	LCARD,LMTD,LMT,
			NO.-of-Element
9	M1	[11,14,15I5]	LCARD,NSET,NO.-&-
			Value-of-Componants
10	M2	[11,14,12,13,1415]	LCARD,NSETD,LN,NSET,
			NO.-of-Elements
11	W	[11,14,13I5]	LCARD,NO.-of-Nodes
12	S1	[3E10.3]	YDATS,UNWTS,HVRAT
13	S2	[6E10.3]	XSTRO,YSTRO,TSTRO,ZSTRO,XZSTR,
			YZSTR
14	LD	[11,14,15,6(11,F9.3)]	LCARD,LD,NODE,NO,-&-
			Value-of-Degree-of-Freedom
15	B1	[11,14,3X.I5,6I2,6F10.3]	LCARD,NSET,NO.-&-
			Value-of-Degree-of-Freedom
16	B2	[11,14,12,13,14I5]	LCARD,NSETD,LN,NSET,
			No.-&-Value-of-Degree-of-Freedom
17	P1	[11,14,3X,6I2,6F10.3]	LCARD,NSET,NO-&-
			Value-of-Degree-of-Freedom
18	P2	[11,14,15,8(I3,I2)]	LCARD,NSET,No-&-
			Value-of-Degree-of-Freedom
19	AD	[I1,F9.3,20I2]	LCARD,NO.-of-Increaments
20	EX	[I1,I4,I5,F10.3]	LCARD,NO.-of-Increament,
			No.-of-Material-
			Property-Set,Excavation-Factor

Remark. *In preparing aa input file, one should ensure that the Data Cardsets are in the right order, and some of them may be omitted. The following list gives the details about the "Optional Data sets".*

(1). The W Cards (set 11), only needed if NBDRY > 0.

(2). The SI Cards (set 12), only needed if NGRIS I ≥ 1.

(3). The S2 Cards (set 13), only needed if NGRIS = 2.

(4). The B1 Cards (set 15), only needed if NBSET ≥ 0.

(5). The B2 Cards (set 16), only needed if NBSET ≥ 0.

(6). The P1 Cards (set 17), only needed if NPSET ≥ 0.

(7). The P2 Cards (set 18), only needed if NPSET ≥ 0.

2.2. Descriptions of the variable names

Now we give a brief description of some important variable names used in **FESTER** with their default values. The variable names are the same as that in the 2-D version but their default values may be different. The default value in the 3D version is the number in the parentheses following the variable. More detailed descriptions of the variable names and their default values for 2-D **FESTER** can be obtained in [13,20,21].

2.2.1. The mesh and load variables

1. NPOIN(-): No. of Nodes in mesh.
2. NELEM(-): No. of Elements in mesh.
3. NFIXV(-): No. of Fixed degrees of freedom in mesh.
4. MSTYP(3): Problem type, set to 3 for 3D problems.
5. NDIME(3): No. of Dimensions (also set to 3).
6. NODEM(20): Max. No. of nodes in an element.
7. NDOFM(3): Max. No. of degrees of freedom per node.
8. NGAUS(2): Order of Gauss quadrature rule.
9. NSTRE(6): No. of stress components.
10. NLAPS(l): Type of analysis: 1 =: for small displacement analysis, 2 =: for large displacement analysis.
11. NEXCA(-): Type of loading; 1 = Nodal Loads, 2 = Stress Removal and 3 = Excavation.
13. NPROS(-): No. of material property sets.
14. NPROP(19): Max. No. of material property components in a sets.

16. NBDRY(-): No. of nodes around the tunnel Boundary.
17. NGRIS(0): Type of *in situ* stress: 0 =: none, 1 =: gravity only and 2 =: gravity & uniform stress.
19. NINCS(1): No. of load increments.
20. NITER(1): Max. No. of timesteps per load increment.
21. NBSET(0): No. of body force sets.
22. NPSET(0): No. of surface traction load sets.

These variables are stored in an array NCONS of length 24 and the integers in front of the variables listed above indicate their positions in the array. For example, NCONS(8) = NGAUS.

2.2.2. The computing control parameters (real)

1. TOLER(0.10): Tolerance control parameter.
2. DTINT(0.0l): Initial timestep Δt_0 .
3. TAUFT(0.0l): Timestep size control parameter τ.
4. FTIME(1.20): Timestep size control parameter F_t.
5. YDMIN(0.00): Yield surface tolerance parameter Y_{min}.
6. ALLOW(10.0): Max. timestep control parameter.
7. TIMEX(0.00): Time integration parameter θ, $\theta = 0$ explicit, $0 < \theta \leq 1$ implicit.
8. FLOWC(0.00): The visco-plasticity flow constant c.

These variables are stored in an array CMISC of length 8 and the integers in front of the variables listed above indicate their positions in the array. For example, CMISC(2) = DTINT. The physical meaning of them are given in [34].

2.2.3. Some other variables

1. LTYPE(-): The element type array. In the 3-D version program:

LTYPE(l) = 62: The ID quadratic joint element;
LTYPE(2) = 31: The linear (2D) element;
LTYPE(3) = 33: The linear (2D) element;
LTYPE(4) = 44: The linear (2D) element;
LTYPE(5) = 63: The quadratic triangular (2D) element;
LTYPE(6) = 54: The infinite quadratic (2D) element;
LTYPE(7) = 84: The 8-noded quadratic (2D) element;

LTYPE(8) = 86: The 8-noded brick (linear,3D) element;

LTYPE(9) = 206: The 20-noded brick (quadratic,3D) element;

LTYPE(I0) = 162: The 2D quadratic joint element;

LTYPE(11) = 126: The 3D infinite (quadratic) element (Type a);

LTYPE(12}= 34: The doubly infinite (2D) element;

LTYPE(13) = 76: The 3D infinite (quadratic) element (Type b);

LTYPE(14) = 46: The 3D infinite (quadratic) element (Type c).

2. LMT(2): The Material type indicator:

LMT = 1: Linear elastic structure (no *in situ* stress);

LMT = 2: Isotropic linear elastic material;

LMT = 3: Orthotropic linear elastic material;

LMT = 4: Isotropic Mohr-Coulomb linear elasto-visco-plastic material;

LMT = 5: Isotropic Hoek-Brown linear elasto-visco-plastic material;

LMT = 6: Isotropic Mohr-Coulomb linear elasto-visco-plastic material;

LMT = 7: Isotropic Hoek-Brown linear elasto-visco-plastic material;

LMT = 8: Isotropic Drucker-Prager linear elasto-visco-plastic material;

LMT = 9: Elastic joint element material.

3. YDATS(-): The depth below the surface $Z = 0$ mesh datum plane.

4. UNWTS(-): The unit weight of the material (rock).

5. HVRAT(l): The lateral stress ratio K_0 [27,34].

6. PROPS(-): The material sets and their property parameters which is explained in details in [27,34].

7. SCONV(-l.0): The Sign Convention for both stresses and strains: SCONV = -1.0 means that compression stresses are defined as positive values.

The meaning of some other variable names employed in the program **FESTER** can be obtained in [13,20,21].

§3. Principal stress and stress invariants analyses

In this section, we derive the formulae for the computation of stress invariants and their first and second derivatives which are used in the program **FESTER.** Some other

related formulae are also provided.

First, the stress tensor $\underline{\sigma}$ is described as a vector of length six:

$$\underline{\sigma} := \left(\sigma_x, \sigma_y, \sigma_z, \tau_{xy}, \tau_{xz}, \tau_{yz}\right)^t \qquad (3,1\})$$

and the strain tensor $\in$ is defined similarly, which will be given explicitly in §5. The principal stresses and strains are denoted by $\sigma_1, \sigma_2, \sigma_3, \left(\sigma_1 \geq \sigma_2 \geq \sigma_3\right)$ and $\in_1, \in_2, \in_3, (\in_1 \geq \varepsilon_2 \geq \varepsilon_3)$ respectively. Then the stress invariants I_1, I_2, I_3 and the deviatoric stress invariants J_2 and J_3 are given by [8,18,29]:

$$\begin{aligned}
I_1 &:= \sigma_x + \sigma_y + \sigma_z, \\
I_2 &:= -\sigma_x\sigma_y - \sigma_x\sigma_x - \sigma_y\sigma_z + \tau_{xy}^2 + \tau_{xz}^2 + \tau_{yz}^2, \\
I_3 &:= \sigma_x\sigma_y\sigma_z - \sigma_x\tau_{yz}^2 + \sigma_y\tau_{xz}^2 + \sigma_z\tau_{xy}^2, \\
J_2 &:= \tfrac{1}{6}[(\sigma_x - \sigma_y)^2 + (\sigma_x - \sigma_z)^2 + (\sigma_y - \sigma_z)^2 + \tau_{xy}^2 + \tau_{xz}^2 + \tau_{yz}^2, \\
&:= I_2 + \tfrac{1}{3}I_1^2, \\
J_3 &:= I_3 + \tfrac{1}{3}I_2I_1 + \tfrac{2}{27}I_1^3.
\end{aligned} \qquad (3,2)$$

Hence, the characteristic equation (stress) is thus given by

$$\sigma^3 - I_1\sigma^2 - I_2\sigma - I_3 = 0. \qquad (3.3)$$

For convenience, we introduce another invariant, an angle θ, which is equivalent to the Lode Angle [21]:

$$cos(3\theta) := \frac{3\sqrt{3}J_3}{2\sqrt{J_2^3}}, \qquad 0 \leq \theta \leq \tfrac{\pi}{3}. \qquad (3.4)$$

It should be stressed that this θ is different from the θ_{OH} defined in Owen & Hinton [21]. They are related by:

$$\theta = \theta_{OH} + \tfrac{\pi}{6}. \qquad (3.5)$$

Then, the principal stresses can be written in a simple formula in terms of these invariants [21,34]:

$$\begin{Bmatrix}\sigma_1\\ \sigma_2\\ \sigma_3\end{Bmatrix} = \tfrac{2\sqrt{J_2}}{\sqrt{3}}\begin{bmatrix}\cos(\theta)\\ \cos(\theta - \frac{2\pi}{3})\\ \cos(\theta + \frac{2\pi}{3})\end{bmatrix} + \tfrac{I_1}{3}\begin{Bmatrix}1\\1\\1\end{Bmatrix}. \qquad (3.6)$$

From these equations and by use of the chain rule, we can obtain the partial derivatives of these invariants and principal stresses $\{\sigma_i\}, i = 1,2,3$ with respect to the stress components $\sigma_x, \sigma_y, \ldots\ldots,$, which will be used in the yield and crack criteria and the flow rules:

$$\frac{\partial\sigma_i}{\partial\underline{\sigma}} = \tfrac{2}{\sqrt{3}}\left[\cos(\theta + \theta_i)\frac{\partial\sqrt{J_2}}{\partial\underline{\sigma}} - \sqrt{J_2}\sin(\theta + \theta_i)\frac{\partial\sigma}{\partial\underline{\sigma}}\right] + \tfrac{1}{3}\frac{\partial I_1}{\partial\underline{\sigma}} \qquad (3.7)$$

where $\theta_1 := 0, \theta_2 := \frac{-2\pi}{3}$ *and* $\theta_3 := \frac{2\pi}{3}$.

From equations in (3.2), the first derivatives of the invariants, with respect to the stress vector $\underline{\sigma}$, could be derived:

$$\frac{\partial I_1}{\partial \underline{\sigma}} = (1,1,1,0,0,0)^{\mathrm{t}},$$

$$\frac{\partial I_2}{\partial \underline{\sigma}} = -(\sigma_y + \sigma_z, \sigma_x + \sigma_z, \sigma_x + \sigma_y, -2\tau_{xy,} - 2\tau_{xz}, -2\tau_{yz})^t,$$

$$\frac{\partial I_3}{\partial \underline{\sigma}} = (\sigma_y\sigma_z - \tau_{yz}^2, \sigma_x\sigma_z - \tau_{xz}^2, \sigma_x\sigma_y - \tau_{xy}^2, -2\sigma_z\tau_{xy} + 2\tau_{xz}\tau_{yz},)$$

$$(-2\sigma_y\tau_{xz} + 2\tau_{xy}\tau_{yz}, -2\sigma_x\tau_{yz} + 2\tau_{xy}\tau_{xz})^t, \qquad (3,8)$$

$$\frac{\partial \sqrt{J_2}}{\partial \underline{\sigma}} = \frac{1}{6\sqrt{\mathrm{J}_2}}(3\frac{\partial I_2}{\partial \underline{\sigma}} + 2I_1\frac{\partial I_1}{\partial \underline{\sigma}}),$$

$$\frac{\partial J_3}{\partial \underline{\sigma}} = \frac{1}{9}(9\frac{\partial I_3}{\partial \underline{\sigma}} + 3I_1\frac{\partial I_2}{\partial \underline{\sigma}} + 3I_2\frac{\partial I_1}{\partial \underline{\sigma}} + 2I_1^2\frac{\partial I_1}{\partial \underline{\sigma}}),$$

$$\frac{\partial \theta}{\partial \underline{\sigma}} = \frac{-\sqrt{3}}{4\sin(3\theta)\sqrt{J_2^5}}(2J_2\frac{\partial J_3}{\partial \underline{\sigma}} - 3J_3\frac{\partial J_2}{\partial \underline{\sigma}}).$$

In the implicit visco-plastic algorithm used in **FESTER** the second derivatives (Hessian Matrices) of invariants $I_2, \sqrt{J_2}, J_3$ and θ are needed to calculate the matrix H. Hence, for completeness, we write out the formulae for the computation of these values for the Drucker-Prager (DP) [21,40] and the Hoek-Brown (HB) [14,22,34] plastic potentials which are defined by the following equations:

$$Q(\underline{\sigma})_{DP} := \sqrt{J_2} - \alpha I_1,$$

$$Q(\underline{\sigma}\,\underline{\sigma})_{HB} := -\frac{m'}{3}I_1 + \frac{3}{\sigma_c}J_2 + \frac{\sqrt{3}m'}{2}\sqrt{J_2} \qquad (3,9)$$

where α and m' the empirical parameter and the dilation parameter respectively. From (3.8), we can obtain

$$\mathrm{M}_{var\,I\,2} := \frac{\partial^2 \mathrm{I}_2}{\partial^2 \underline{\sigma}} = \begin{pmatrix} 0 & 1 & 1 & 0 & 0 & 0 \\ 1 & 0 & 1 & 0 & 0 & 0 \\ 1 & 1 & 0 & 0 & 0 & 0 \\ 0 & 0 & 0 & -2 & 0 & 0 \\ 0 & 0 & 0 & 0 & -2 & 0 \\ 0 & 0 & 0 & 0 & 0 & -2 \end{pmatrix} \qquad (3,10)$$

and

$$\mathrm{M}_{ste\,f\,f} := \frac{\partial^2 \sqrt{J_2}}{\partial^2 \underline{\sigma}} = \frac{1}{\sqrt{J_2}}\frac{\partial \sqrt{J_2}}{\partial \underline{\sigma}}(\frac{\partial \sqrt{J_2}}{\partial \underline{\sigma}})^t + \frac{1}{6\sqrt{J_2}}\mathrm{M}_{const} \qquad (3.11)$$

where $\mathrm{M}_{\mathrm{const}}$ is a constant matrix

$$\mathrm{M}_{const} := \begin{pmatrix} 2 & -1 & -1 & 0 & 0 & 0 \\ -1 & 2 & -1 & 0 & 0 & 0 \\ -1 & -1 & 2 & 0 & 0 & 0 \\ 0 & 0 & 0 & 6 & 0 & 0 \\ 0 & 0 & 0 & 0 & 6 & 0 \\ 0 & 0 & 0 & 0 & 0 & 6 \end{pmatrix} \qquad (3.12)$$

The Hessian matrices of I_3, J_3 and θ are given by

$$\mathrm{M}_{varI3} := \begin{pmatrix} 0 & \sigma_z & \sigma_y & 0 & 0 & -2\tau_{yz} \\ \sigma_z & 0 & \sigma_x & 0 & -2\tau_{xz} & 0 \\ \sigma_y & \sigma_x & 0 & -2\tau_{xy} & 0 & 0 \\ 0 & 0 & -2\tau_{xy} & -2\tau_z & 2\tau_{yz} & 2\tau_{xz} \\ 0 & -2\tau_{xz} & 0 & 2\tau_{yz} & -2\sigma_y & 2\tau_{xy} \\ -2\tau_{yz} & 0 & 0 & 2\tau_{xz} & 2\tau_{xy} & -2\sigma_x \end{pmatrix}, \tag{3.13}$$

$$\mathrm{M}_{varJ3} := \mathrm{M}_{varI3} + \frac{1}{3}\,\mathrm{M}_{varI2} + \frac{\partial I_2}{\partial Q}\left(\frac{\partial I_1}{\partial Q}\right)^t + \frac{\partial I_1}{\partial Q}\left(\frac{\partial I_2}{\partial Q}\right)^t - \frac{4}{9} I_1 \frac{\partial I_2}{\partial Q}\left(\frac{\partial I_1}{\partial Q}\right)^t \tag{3.14}$$

and

$$\begin{aligned} \mathrm{M}_{\mathrm{var}\theta} = {} & \frac{-\sqrt{3}}{2\sin 3\theta \sqrt{\mathrm{J}_2^3}} \frac{\partial^2 J_3}{\partial^2 \underline{\sigma}} - \frac{\cos 3\theta}{\sin 3\theta} \frac{\partial \theta}{\partial \underline{\sigma}} \left(\frac{\partial \theta}{\partial \underline{\sigma}}\right)^t \\ & + \frac{3\sqrt{3}}{2J_2^2 \sin 3\theta} \left[\frac{\partial J_3}{\partial \underline{\sigma}} \left(\frac{\partial \sqrt{J_2}}{\partial \underline{\sigma}}\right)^t + \frac{\partial \sqrt{J_2}}{\partial \underline{\sigma}} \left(\frac{\partial J_3}{\partial \underline{\sigma}}\right)^t \right] \\ & - \frac{6\sqrt{3} J_3}{\sqrt{J_2^5} \sin 3\theta} \frac{\partial \sqrt{J_2}}{\partial \underline{\sigma}} \left(\frac{\partial \sqrt{J_2}}{\partial \underline{\sigma}}\right)^t + \frac{3\sqrt{3}\mathrm{J}_3}{2J_2^2 \sin 3\theta} \frac{\partial^2 \sqrt{J_2}}{\partial^2 \underline{\sigma}}. \end{aligned} \tag{3.15}$$

For the Drucker-Prager plastic potential, the flow vector b_{DP} and its derivatives v_{DP} are given by

$$\begin{aligned} b_{DP} &:= \frac{\partial Q_{DP}}{\partial \underline{\sigma}} = \frac{\partial \sqrt{J_2}}{\partial \underline{\sigma}} - \alpha \frac{\partial I_1}{\partial \underline{\sigma}}, \\ v_{DP} &:= \frac{\partial b_{DP}}{\partial \underline{\sigma}} = \frac{\partial^2 \sqrt{J_2}}{\partial^2 \underline{\sigma}}. \end{aligned} \tag{3.16}$$

For the Hoek-Brown plastic potential plastic potential, the flow vector b_{HB} and its derivatives v_{HB} are given by

$$\begin{aligned} b_{HB} &:= \frac{\partial Q_{HB}}{\partial \underline{\sigma}} = -\frac{m'}{3} \frac{\partial I_1}{\partial \underline{\sigma}} + \frac{6\sqrt{J_2}}{\sigma_c} \frac{\partial \sqrt{J_2}}{\partial \underline{\sigma}} + \frac{\sqrt{3} m'}{2} \frac{\partial \sqrt{J_2}}{\partial \underline{\sigma}}, \\ v_{HB} &:= \frac{\partial^2 Q_{HB}}{\partial^2 \underline{\sigma}} = \frac{6\sqrt{J_2}}{\sigma_c} \frac{\partial^2 \sqrt{J_2}}{\partial^2 \underline{\sigma}} + \frac{6\sqrt{J_2}}{\sigma_c} \frac{\partial \sqrt{J_2}}{\partial \underline{\sigma}} \left(\frac{\partial \sqrt{J_2}}{\partial \underline{\sigma}}\right)^t + \frac{\sqrt{3} m'}{2} \frac{\partial^2 \sqrt{J_2}}{\partial^2 \underline{\sigma}} \end{aligned} \tag{3 17}$$

Finally, for computational purposes, we give the formulae of the Hessian matrices (second order derivatives with respect to the Cartesian stress components $\{\sigma_x, \sigma_y, ...\}$) of the principal stresses $\{\sigma_i\}, i = 1,2,3$. These formulae come from (3.6) and (3.7) directly.

$$\begin{aligned} \frac{\partial^2 \sigma_i}{\sigma} = {} & \frac{2}{\sqrt{3}} \left\{ \cos(\theta + \theta_i) \frac{\partial^2 \sqrt{J_2}}{\partial^2 \sigma} - \sin(\theta + \theta_i) \left[\frac{\partial \sqrt{J_2}}{\partial \sigma} \left(\frac{\partial \theta}{\partial \sigma}\right)^t + \frac{\partial \theta}{\partial \sigma} \left(\frac{\partial \sqrt{J_2}}{\partial \sigma}\right)^t \right] \right\} \\ & + \frac{2\sqrt{J_2}}{\sqrt{3}} \sin(\theta + \theta_i) \frac{\partial^2 \theta}{\partial^2 \underline{\sigma}}, i = 1,2,3. \end{aligned} \tag{3.17}$$

All these invariants and their derivatives are programmed in the 3D version **FESTER** subroutine **INVAR**. Modifications to other related subroutines are also made consistently.

§4. **2D joint element (surface contact)**

A 2D joint element (surface contact) is introduced in the 3D version of **FESTER** to simulate the sliding and fracturing (with or without gaps) of rock movement during tunnel excavation. This joint element is similar to the 1D/2D/3D joint element described in [2,12,28,35] in theory. However, it has zero thickness and allows opening. In **FESTER** the ID joint element is constructed from a pair of 3-noded bar elements; by contrast, the 2D-joint element consists of a pair of 8-noded quadratic is oparametric element5(see Figure 4.1). Hence a 2D joint element in **FESTER** has sixteen nodes. Other joint elements with more or less nodes can also be formulated similarly.

4.1, Formulation of the 2D joint element-surface contact modelling

The mathematical formulation of the (element) "stiffness matrix" and "B—matrix", (i.e., the strain-displacement relation matrix) of the 16-noded joint element without *opening,* (or bonded element) is as follows. The opening problem will be discussed in the next subsection. For simplicity, we first consider a special case of joints—the joint element is parallel to the *x-y* plane during the process of deformation. The general sliding cases, in which the joint element deforms arbitrarily, will be studied at the end of this subsection.

First, we need some notation. Let d := $(u,v,w)^t$ denote the displacement at any point in the joint element, d_j^0 be the displacement of the j-th node, j = 1,2,..., 16; and Δs denote the relative displacement (slip) at any point on the upper side of the joint element, and $\Delta s^0{}_i$ denote the slip at the i-th node on the Upper Side of the element (see Figure 4.1), i = 1,2,...,8. That is,

$$\Delta s_i^0 := d_i^0 - d_{i+n}^0 \tag{4.0}$$

The functions, $\phi_i, i = 1,2,...,8,$ are the (isoparametric) shape functions of the (2D) 8- noded quadratic elements (In general 2D joint elements, we shall use *2n* to denote the number nodes in the element. Hence, in our special case, n = 8.). Furthermore, we assume, just as in finite element methods that

$$\Delta s = \sum_{i=1}^{n} \Delta s_i^0 \phi_i := N \Delta S_0, \tag{4.1}$$

where, I is the 3×3 identity matrix and

$$N := (\phi_1 I, \phi_2 I, ..., \phi_n I) \quad \in R^{3n}, \tag{4.2}$$

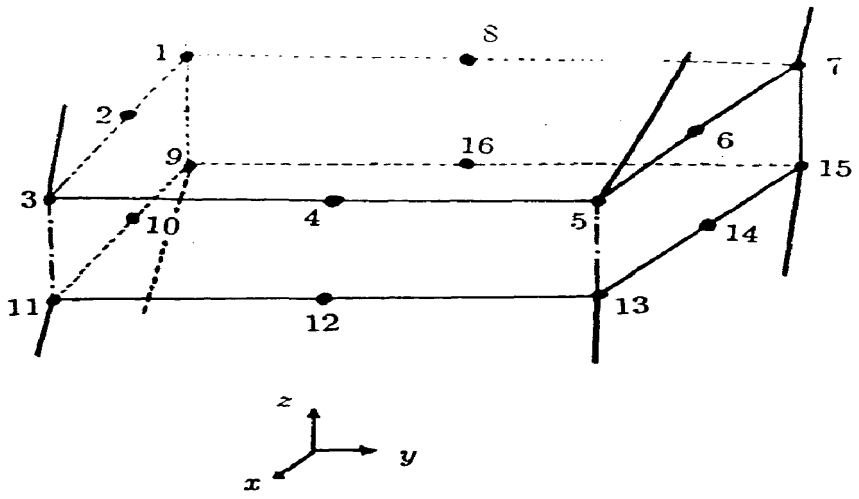

Figure 4.1. A 2D joint element parallel to the *x-y* plane.

and

$$\Delta S_0 := (\Delta S_1^0, \Delta S_2^0, ..., \Delta S_n^0)^t \quad \in R^{3n}. \tag{4.3}$$

Then the virtual External Work, δE_{ext} is given by [2,12]:

$$\delta E_{ext} = \delta \Delta S_0^t \Delta_P \tag{4.4}$$

where Δp is the *Nodal Force* vector of length 3n. While the *Virtual Strain Energy (Shear Work), δE_{shr},* is given by [2,12,28,35]:

$$\delta E_{shr} = a^2 \int_{\Omega} \underline{\tau}^t \, \delta \Delta s d\Omega, \tag{4.5}$$

where, $\underline{\tau}$ is the stress vector in the joint element (the contact surface). Here, $\underline{\tau} := (\tau_x, \tau_y, \tau_{xy})^t \in R^3$, since other stress components of $\underline{\tau}$ are definitely zeros. The contact region is denoted by Ω and α is a material constant. By assuming the following *stress-slip relations,* which comes from experiments [2,12,28,35]:

$$\underline{\tau} = G\Delta s, \quad G \in R^{3\times 3}, , \tag{4.6}$$

for some diagonal matrix G = *diag(K_{sx}, K_{sy}, K_{nz}),* here K_{sx} and K_{sy} are the elastic (friction) moduli in the *x* and y directions (or in general, two directions in the tangent plane) *(K_{sx} and K_{sy}* are assumed to have the same value in the program FESTER) and

K_{nz} is the normal elastic modulus of the joint element *(K_{nz}* is set to be 10^{20} in **FESTER** for convenience, the details of these values will be discussed in the next subsection), then we have:

$$\begin{aligned}\delta E_{shr} &= a^2 \int_\Omega \underline{\tau}^t \, \delta\Delta s d\Omega \\ &= a^2 \int_\Omega \delta\Delta s^t G \Delta s d\Omega \\ &= a^2 \delta\Delta S_0^t \left(\int_\Omega N^t G N d\Omega\right) \Delta S_0. \end{aligned} \tag{4.7}$$

From the *Virtual Work Principle:*$\delta E_{shr} = \delta E_{ext}$, we have, in the state of equilibrium:

$$\Delta_P = a^2 \left(\int_\Omega N^t G N d\Omega\right) \Delta S_0 \equiv K_{sol} \Delta S_0, \tag{4.8}$$

where, K_{sol} is a kind of element *stiffness matrix* defined by

$$K_{sol} := \int_\Omega N^t G N d\Omega \quad \in R^{3n\times 3n} \tag{4.9}$$

Now, let $D_0 \in R^{6n\times 6n}$ denote the vector of displacements at the sixteen nodes ($2n$) of the joint element, then we can easily find that there is a *difference matrix* $Z \in R^{3n\times 6n}$ such that (4.0) can be written

$$\Delta S_0 \equiv Z D_0, \tag{4.10}$$

where, the matrix Z is characterized by $Z_{3i+1,3i+1} = 1, Z_{3i+1,3n+3i+1,} = -1 \; \forall i \geq 0$ and the other elements = 0. Therefore, we can obtain the following *Force-Displacement* relation for the joint element:

$$\Delta p = K_{sol} Z D_0. \tag{4.11}$$

However, we can formulate the δE_{ext} in the following way:

$$\delta E_{ext} = \delta S_0^t \Delta p \equiv \delta D_0^t P, \tag{4.12}$$

where, $p \in R^{6n}$ is the nodal force vector at the sixteen nodes ($2n$) of the joint element. Combining this with (4.10), one obtains

$$p = Z^t \Delta p. \tag{4.13}$$

From equations (4.8), (4.10) and (4.13), the following *Nodal Force—Nodal Displacement* relation can be derived:

$$\mathbf{p} = \mathbf{Z}^t \mathbf{K}_{sol}\mathbf{Z}\mathbf{D}_0 \equiv \mathbf{K}_{jnt}\,\mathbf{Do}, \tag{4.14}$$

with the *stiffness matrix* $\boldsymbol{K}_{jnt}$ of the joint element given by

$$\boldsymbol{K}_{jnt} := \mathbf{Z}^t \mathbf{K}_{sol}\mathbf{Z}. \tag{4.15}$$

Furthermore, we can also form the *B-matrix,* $\mathbf{B}_{jnt}$, and the *D-matrix,* $\mathbf{D}_{jnt}$, for the joint element:

$$\begin{aligned}\mathbf{B}_{jnt} &= \mathbf{NZ} \\ &= \left(\phi_1 \mathrm{I}, \phi_2 \mathrm{I}, ..., \phi_n \mathrm{I}, -\phi_1 \mathrm{I}, -\phi_2 \mathrm{I}, ..., -\phi_n \mathrm{I},\right)\end{aligned} \tag{4.16}$$

and

$$\mathbf{D}_{jnt} := \mathbf{G} \equiv \begin{pmatrix} K_{SX} & 0 & 0 \\ 0 & K_{Sy} & 0 \\ 0 & 0 & K_{nz} \end{pmatrix}. \tag{4.17}$$

Therefore, the *stiffness matrix* for the joint element can also be written in the following form:

$$\mathbf{K}_{jnt} := \int_{\Omega} \mathbf{B}^t_{jnt} \mathbf{D}_{jnt} \mathbf{B}_{jnt}\, d\Omega. \tag{4.18}$$

In general, we can also formulate in a similar way that the *B-matrix* and *D-matrix* for 2D joint elements in space (cf. Figure 4.2) is given by:

$$\mathbf{B}_{jnt} = \mathbf{Q}^t(\mathbf{N}, -\mathbf{N}) = \mathbf{Q}^t\mathbf{NZ}, \tag{4.19}$$

and

$$\mathbf{D}_{jnt} := \begin{pmatrix} K_{st_1} & 0 & 0 \\ 0 & K_{st_2} & 0 \\ 0 & 0 & K_{ns} \end{pmatrix}. \tag{4.20}$$

where, $\mathrm{K}_{\mathrm{st}_1}$ and $\mathrm{K}_{\mathrm{st}_2}$ are the elastic (friction) moduli in two orthogonal directions in the tangent plane, and K_{nz} is elastic modulus in the normal direction of the joint element. For isotropic materials, we have

$$K_{st_1} = K_{sz},\ K_{st_{21}} = K_{sy},\ K_{ns} = K_{nz}. \tag{4.21}$$

This is assumed in **FESTER** for convenience. More about the D-matrix will be given later.

The matrix **Q** in (4.19) is an orthogonal (rotation) matrix that transforms the original coordinates system xyz to a cartesian coordinates system $x'y'z'$ with the new z' axis in the direction of the surface normal at that point (i.e., the Frenet frame). More explicitly, the rotation matrix **Q** is given by:

$$\mathbf{Q}:=(\mathrm{q}_1,\mathrm{q}_2,\mathrm{q}_3). \tag{4.22}$$

The vector $\mathbf{q_3}$ is the (unit) normal vector of the joint element surface at the point (x, y, z) (local coordinates (ξ,η,ζ)) and $\mathbf{q_1}$ and $\mathbf{q_2}$ are (unit) vectors in the tangent plane of the element:

$$\begin{aligned} \mathrm{q}_1 &:= \mathrm{v}_4 \times \mathrm{q}_3, \\ \mathrm{q}_2 &:= \mathrm{q}_1 \times \mathrm{q}_3. \end{aligned} \tag{4.23}$$

The vector $\mathbf{v_4}$ is defined as either $(1,0,0)^t$ or $(0,1,0)^t$, which depends on the normal direction of the contact surface at that point. More explicitly,

$$\mathbf{v}_4 = \begin{cases} (1,0,0)^t, & \text{if } v_1 \neq (1,0,0)^t, \\ (0,1,0)^t, & \text{if } v_1 = (1,0,0)^t, \end{cases} \tag{4.24}$$

where

$$\begin{aligned} \mathbf{v}_1 &:= \left(\frac{\partial x}{\partial \xi}, \frac{\partial y}{\partial \xi}, \frac{\partial z}{\partial \xi}\right)^t, \\ \mathbf{v}_2 &:= \left(\frac{\partial x}{\partial \eta}, \frac{\partial y}{\partial \eta}, \frac{\partial z}{\partial \eta}\right)^t \end{aligned} \tag{4.25}$$

and

$$\mathbf{q}_3 := \frac{\mathbf{v}_1 \times \mathbf{v}_2}{\|\mathbf{v}_1 \times \mathbf{v}_2\|}. \tag{4.26}$$

The element stiffness matrix, $\mathbf{K}_{jnt}$, is still given by (4.18) together with the B-matrix and D-matrix given by (4.19) and (4.20).

In formula (4.26), the vector q_3 is the unit normal vector of the joint surface. In general, the vector is unique at any point on the joint element so that the vectors $\mathbf{v_1}$ and $\mathbf{v_2}$ cannot vanish at any point. Hence, (2.26) is always meaningful.

Remark 4.1. Although the B-matrix and stiffness matrix for 16-noded 2D-joint elements are formulated here, the results obtained in this section could be generalised to other 2D joint elements. For example, by changing the node number n and the shape functions $\{\phi_i\}, i = 1,2, \ldots,n$, then its corresponding stiffness matrix and B-matrix are given by (4.18) and (4.16) respectively.

Remark 4.2. In FESTER the 1D and 2D joint elements are treated as special 2D and 3D elements respectively. Since there is no extra node introduced in the mesh, that is,

no node in the mesh belongs to a joint element only, the global stiffness matrix can be assembled from element stiffness matrices directly. Hence, the displacement, vector can be obtained by solving the system of equations of equilibrium.

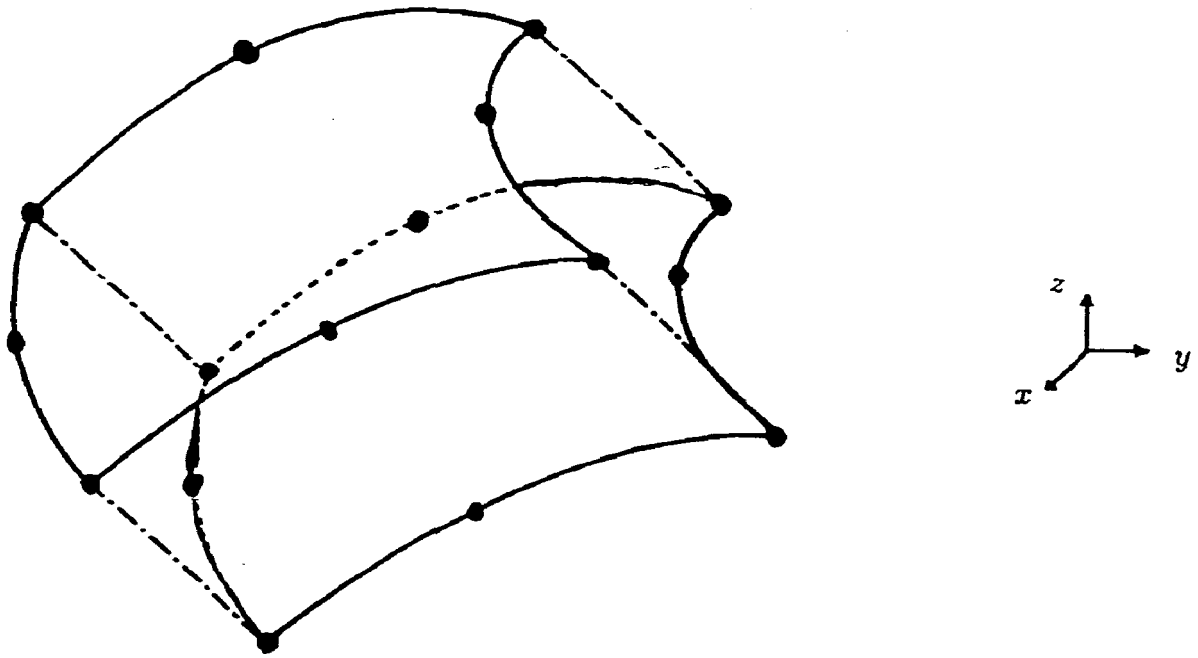

Figure 4.2. A general 2D joint element in the *x-y-z* system.

4.2. Gaps in joint elements and control parameters

In this subsection, we discuss another characteristic of joint elements: convergence and separation. This property of joint elements could be used to simulate discontinuities in rock masses and other materials. As in Beer's formulation for general joint (shell) elements [2], it can be shown that the B-matrix and the element stiffness matrix for the 2D joint element are still given by (4.16) (or (4.19) in general) and (4.18) respectively. This can be derived by the standard procedure of minimising the total potential energy [2]. Hence, we only state here some of the parameters used in dealing with joint elements and their physical background..

A. *D-matrix for joint elements:* $\mathbf{D}_{int}$

The matrix $\mathbf{D}_{\mathbf{int}}$ in (4.20) characterises the sliding and separation/convergence properties of joint elements. Its diagonal elements have a very clear physical explanation. K_{st_1} and K_{st_2} are the elastic (friction) moduli in two orthogonal directions in the tan-

gent plane of the contact point, and K_{nz} is elastic modulus in the normal direction of the joint element (the convergence and separation control). For isotropic materials, we have, compared with (4.17):

$$K_{st_1} = K_{sx} = K_{st_2} = K_{sy}. \tag{4.27}$$

The actual values of these elastic muduli depend on the material. This special form of D-matrix is a simplification (linearisation) of the stress-strain relation in joint elements. In fact, the relations between the shear stresses and the slips are quite complicated [12] and we will not discuss it further.

B. *The convergence /separation control parameter:* K_{ns}

A convergence and separation option of the 2D joint element is provided by the control parameter: K_{ns}. Here, *convergence* means that the two sides of the element moves closer to each other since it can be treated as a thin shell element [2] with zero thickness while *separation* just means that they move further away from each other. This type of element can be used to model the deformation of the joining of two rock strata in the following two ways. One is a "convergence" modelling $K_{ns} := \infty$, in **FESTER,** $K_{ns} := 10^{20}$), *i.e.,* the two rock strata remain in contact during the process of deformation, which is quite restrictive to model the natural rock contact problem. The other is a "separation" modelling ($0 \le K_{ns} < \infty$) that is, the two rock strata can move arbitrarily, which is a natural modelling of rock joint deformation in practice. The latter is more difficult to be applied in practice than the first one since it allows discontinuities to occur in a continuum which cannot be dealt with by ordinary Finite Element Methods (FEM). This difficulty can be overcome by using some techniques such as *Discrete-Finite Element Methods* (DFEM). Here, we will not discuss DFEM further.

In the present version of **FESTER,** the value of the parameter K_{ns} is restricted to ∞ only. That is, $K_{ns} = 10^{20}$, which means that the element is rigid in the normal direction and elastic in the tangent plane, neither further-convergence nor separation is allowed, only sliding can occur. Other values of K_{ns} will be considered and implemented soon.

For completeness, we list the physical meaning of other values of this control parameter K_{ns}.

i. $0 \le K_{ns} < 10^{20}$: the element is an elastic 3D element, sliding, separation, and convergence (up to zero thickness of the element) as well, are allowed.

ii. Small value of K_{ns} means that the element is an elastic 3D element, which is very soft in the normal direction, sliding, separation and convergence (up to zero thickness of

the element) are allowed.

iii. Large value of K_{ns} means that the element is an elastic 3D element, which is very *hard* in the normal direction, sliding, separation and very small convergence (up to zero thickness of the element) are allowed.

C. *Remarks*

Remark 4.3. *In the present version of* **FESTER** *the 1D and 2D joint elements always have zero thickness, so further convergence or separation cannot happen, only sliding in the joint is allowed.*

Remark 4.4. *To model the fracturing process of rock masses or other solid materials, more general 1D/2D joint elements (non-linear elastic or plastic) should be introduced which may allow "negative thickness" to model collisions between two elastic or elasto-plastic objects. This generalisation of joint elements needs the theory and techniques of DFEM which will not be discussed here.*

Remark 4.5. *In* **FESTER,** *the D-matrix for the 2D joint element given by (4.20) is ated as a constant matrix during the process of deformation for simplicity. In fact,* $\mathbf{D}_{jnt}$ *depends not only on the materials, but also on the values of slips or shear stresses. That is, for real materials, the relations between shear (friction) stresses and slips are non-linear and quite complicated [12]. Hence, to increase accuracy, the non-linear terms in the stress-slip relations should be considered, which may lead to the introduction of non-zero off diagonal elements in* $\mathbf{D}_{jnt}$ *This can be implemented easily to the 3D version* of **FESTER.**

Remark 4.6. *For real materials, there are at least four independent joint parameters: three elastic moduli of the joint* $K_{st_1}(K_{st_2})$, K_{sn} *and the strength values of the joint* σ_{crt_n} *(normal strength, which may be negligible) and* $\sigma_{\mathrm{crt},1}(\sigma_{\mathrm{crt},2})$ *(shear strength, which depends on the angle of friction* ϕ_{jnt} *and the cohesion parameter* C_{jnt}*) [12]. There are many factors influencing these joint parameters: the contact area, the perpendicular aperture distribution and amplitude, the roughness of the two sides of the joint, inclination of apertures, cohesion due to interlocking etc.*

§5. Stress-strain analysis, plane of weakness and cracking

For each of the element types described in §2.2.3, one of the following material models is associated (joint element is restricted to model 9 only):

1. Linear elastic structure (no *in situ* stress in gravity loading);
2. Isotropic linear elastic rock;
3. Orthotropic linear elastic rock;
4. Isotropic elastic-plastic rock with Mohr-Coulomb failure surface;
5. Isotropic elastic-plastic rock with Hoek-Brown failure surface;
6. Orthotropic elastic-plastic rock with Mohr-Coulomb failure surface;
7. Orthotropic elastic-plastic rock with Hoek-Brown failure surface;
8. Isotropic elastic-plastic rock with Drucker-Prager failure surface;
9. Elastic joint (2D) interface in rock.

The material property parameters (nineteen parameters in all) required for these models are listed in table 2.1 in Pan & Reed (cf. [27]).

5.1. Stress-strain analysis of Orthotropic materials

The constitutive law for orthotropic materials, of which the orientation of the out-of-plane-of-weakness-direction is in the z direction (see Figure 5.1), is given by the following relations [17,21,40]:

$$\underline{\sigma} = \mathbf{D}\,\underline{\varepsilon}, \tag{5.1}$$

where

$$\begin{aligned} \underline{\varepsilon} &:= \left(\varepsilon_x, \varepsilon_y, \varepsilon_z, \gamma_{xy}, \gamma_{xz}, \gamma_{yz}\right)^t, \\ \underline{\sigma} &:= \left(\sigma_x, \sigma_y, \sigma_z, \tau_{xy}, \tau_{xz}, \tau_{yz}\right)^t \end{aligned} \tag{5.2}$$

and

$$\mathbf{D} := \begin{pmatrix} C_n(1-v_2^2 C_n) & C_n v_2(1+v_1) & C_n(v_1+v_2^2) & 0 & 0 & 0 \\ C_n v_2(1+v_1) & 1-v_2^2 & C_n v_2(1+v_1) & 0 & 0 & 0 \\ C_n(v_1+v_2^2) & C_n v_2(1+v_1) & C_n(1-v_2^2 c_n) & 0 & 0 & 0 \\ 0 & 0 & 0 & \frac{E_1}{2(1+v_1)} & 0 & 0 \\ 0 & 0 & 0 & 0 & G_2 & 0 \\ 0 & 0 & 0 & 0 & 0 & G_2 \end{pmatrix} \tag{5.3}$$

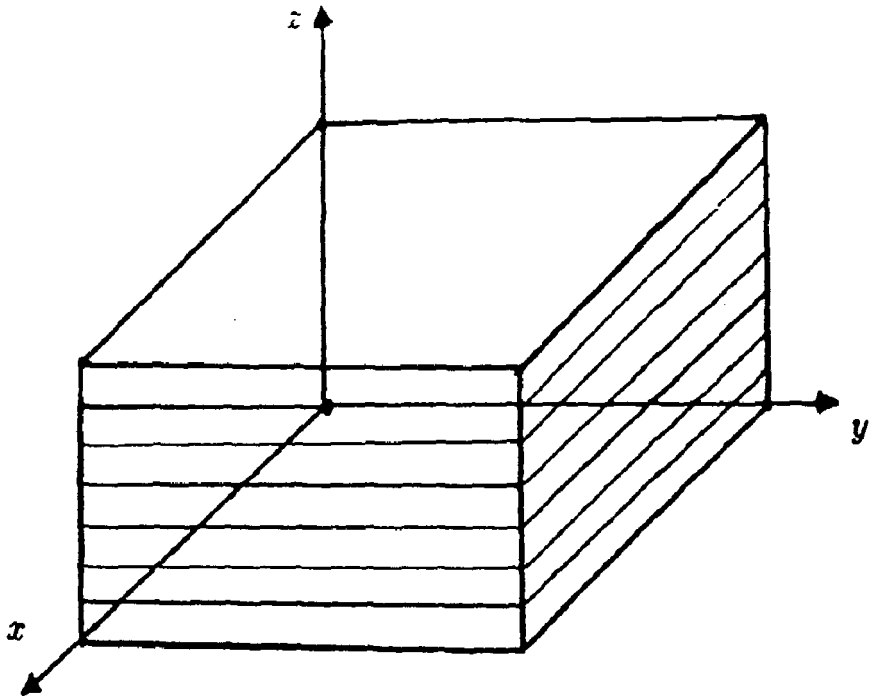

Figure 5.1. An orthotropic material and its (ortho-)coodinate system.

Here, E_1 ,v_1 are the Young's modulus and Poison's ratio in the plane of isotropy (which is parallel to the *x-y* plane) and E_2 ,v_2 ate the corresponding property parameters in the direction normal to the the plane *(z* direction), G_2 is the shear modulus in the normal direction and the constant $C_n := \frac{E_1}{E_2}$. It should be noticed that in the strain vector $\underline{\varepsilon}$ the shear strains $\gamma_{xy},\gamma_{xz},\gamma_{yz}$ are used, not $\varepsilon_{xy},\varepsilon_{xz},\varepsilon_{yz}$. They are related by

$$\gamma_{xy} = 2\varepsilon_{xy}, \gamma_{xz} = 2\varepsilon_{xz}, \gamma_{yz} = 2\varepsilon_{yz}. \tag{5.4}$$

This will be used in the formulation of strain energy and stress (strain) transformation

For isotropic materials, the constitutive law is also given by (5.1)—(5.3) with the property parameters satisfying

$$E_1 = E_2 = E, v_1 = v_2 = v, G_2 = G = \frac{E}{2(1+v)}. \tag{5.5}$$

In this case, the material has only two property parameters, the Young's modulus E and the Poisson's ratio v.

For inclined orthotropic materials, *i. e.,* inclined rock strata, the strain-displacement relation matrix, which is denoted by **D'** now, can be written in the following form [17,40]:

$$\mathbf{D'} = \mathbf{TDT}^t \tag{5.6}$$

where **T** is the *strain transformation matrix* satisfying:

$$\underline{\varepsilon}^{ortho} = \mathbf{T}^t \, \underline{\varepsilon}^{xyz} \tag{5.7}$$

i.e., the matrix T is a coordinates transformation matrix for strain tensors which is defined explicitly by

$$\mathbf{T} := \begin{pmatrix} l_1^2 & m_1^2 & n_1^2 & 2l_1m_1 & 2n_1m_1 & 2l_1n_1 \\ l_2^2 & m_2^2 & n_2^2 & 2l_2m_2 & 2n_2m_2 & 2l_2n_2 \\ l_3^2 & m_3^2 & n_3^2 & 2l_3m_3 & 2n_3m_3 & 2l_3n_3 \\ l_1l_2 & m_1m_2 & n_1n_2 & l_1m_2+l_2m_1 & n_1m_2+n_2m_1 & l_1n_2+l_2n_1 \\ l_2l_3 & m_2m_3 & n_2n_3 & l_2m_3+l_3m_2 & n_2m_3+n_3m_2 & l_2n_3+l_3n_2 \\ l_2l_3 & m_2m_3 & n_2n_3 & l_1m_3+l_3m_1 & n_1m_3+n_3m_1 & l_1n_3+l_3n_1 \end{pmatrix} \tag{5.8}$$

and the vectors $x' := (l_1,\ l_2,\ l_3\ )$,y' := $(m_1,\ m_2,\ m_3\ )$ and $z' := (n_1,\ n_2,\ n_3\ )$, are the directions (unit vectors) of orthotropy in the global coordinates system (x,y,z) as shown in Figure 5.2, and $\underline{\varepsilon}^{ortho}$ and $\underline{\varepsilon}^{xyz}$ denote the strain vectors ($\in \mathbf{R}^6$) in the orthotropic coordinate system (local) and the *xyz* coordinate system respectively.

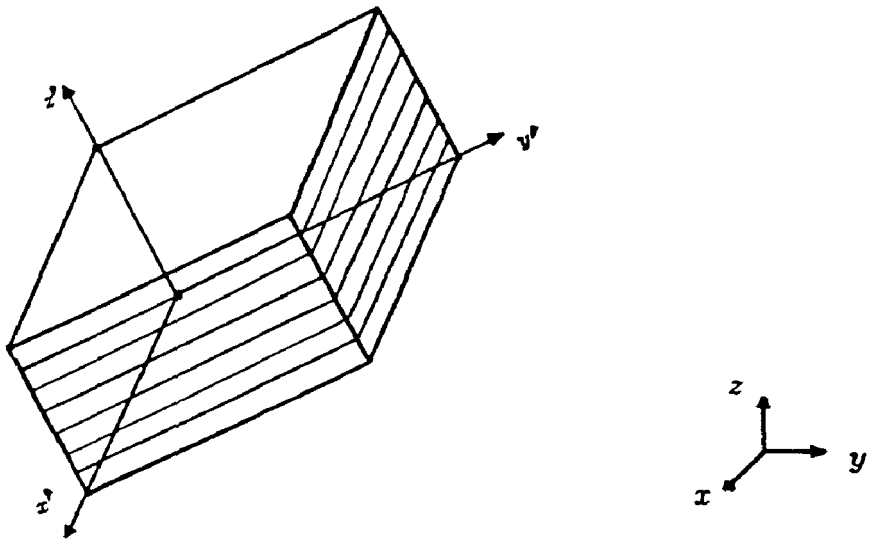

Figure 5.2. An orthotropic material in the *x-y-z* coodinate system.

5.2. Plane of weakness in orthotropic materials and cracking

The plane of weakness arises from the laminated nature of the rock stratum, created during sedimentation [3,4,6]. In the 3D case, the isotropic plane in the rock mass is, in general, spanned by two orthogonal unit vectors, namely $x' := (l_1,\ l_2,\ l_3\ )$ and $y' :=$

(m_1, m_2, m_3). For convenience, the third unit vector, $z' := (n_1, n_2, n_3)$, is introduced so that x'-y'-z' forms a right-hand coordinate system which is called the orthotropic coordinate system. From the above formulation in the previous sub-section, we can easily obtain the normal and shear stresses along the plane of weakness (the x'-y' plane):

$$\begin{Bmatrix} \sigma'_{z'} \\ \tau'_{x'z'} \\ \tau'_{y'z'} \end{Bmatrix} = \begin{bmatrix} l_3^2 & m_3^2 & n_3^2 & 2l_3m_3 & 2n_3m_3 & 2l_3n_3 \\ l_2l_3 & m_2m_3 & n_2n_3 & l_2m_3 + l_3m_2 & n_2m_3 + n_3m_2 & l_2n_3 + l_3n_2 \\ l_2l_3 & m_2m_3 & n_2n_3 & l_1m_3 + l_3m_1 & n_1m_3 + n_3m_1 & l_1n_3 + l_3n_1 \end{bmatrix} \sigma . \tag{5.9}$$

Hence the resultant shear stress τ_{rst} and the normal stress o_n on the plane of weakness are given by

$$\begin{aligned} \tau_{rst} &= \sqrt{\tau'^2_{x'z'} + \tau'^2_{y'z'}}, \\ \sigma_n &= \sigma'_{z'}. \end{aligned} \tag{5.10}$$

We now consider the circumstances in which sliding occurs along the plane of weakness. From the theory of limiting friction [6,12,28,34], sliding occurs if the maximum shear stress τ_{rst} in the plane satisfies the Mohr-Coulom-criterion:

$$\left|\tau_{rst}\right| \geq \sigma_n tan(\varphi_j) + c_j \tag{5.11}$$

where ϕ_j is the angle of friction and C_j *is* the cohesion parameter associated with the joining. Another criterion is that the rock cannot support a tensile stress across the joints, *i. e.,* the rock will break if $\sigma_n < 0$. These formulations are used in **FESTER** to analyse orthotropic materials and joint element sliding. Thus, two more yield functions, and their corresponding flow rules as well, are introduced in **FESTER** to deal with the plane of weakness. The no-slip criterion has yield function $F_1(\underline{\sigma})$ and plastic potential $Q_1(\underline{\sigma})$ defined by

$$\begin{aligned} F_1(\underline{\sigma}) &:= \left|\tau_{rst}\right| - \sigma_n tan(\varphi_j) - c_j, \\ Q_1(\underline{\sigma}) &:= \left|\tau_{rst}\right| - \sigma_n tan(\psi_j) \end{aligned} \tag{5.12}$$

where ψ_i is the angle of dilation. The no-tension criterion has yield function $F_2(\underline{\sigma})$ and plastic potential $Q_2(\underline{\sigma})$ defined as

$$F_2(\sigma) = Q_2(\underline{\sigma}) := -\sigma_n . \tag{5.13}$$

The conventional flow rule is still used in both no-slip and no-tension cases, *i. e.,*

$$\underline{\varepsilon}^i_{vp} = \gamma_j < \Phi(F_i) > + \frac{\partial Q_i(\underline{\sigma})}{\partial \underline{\sigma}}, \qquad i = 1,2 \tag{5.14}$$

where γ_j is the fluidity parameter for the joining and the function notation $< x >+$ is the standard truncated function:

$$< x >_+ := \begin{cases} x, & x \geq 0, \\ 0, & x < 0. \end{cases} \tag{5-15}$$

There are in all four independent yield criteria used in **FESTER.** One of them is used for general rock masses which may be denned as isotropic rock while another two are designed for the test on the plane of weakness. In **FESTER,** the rock cracks on the plane of weakness if either of these two flow rules in (5.12) and (5.13) become active. This cracking process is independent of the the plastic yield of the plastic rock mass. That is, at a given Gauss point, the rock may have been cracked but not yielded plastically, or vice versa, or neither, or both. The last yield criterion, for "isotropic rock masses", used in **FESTER** to model realistic rock behaviour and to cure the instability of the numerical results that may arise during computations is the limited-tensile yield rule, with its plastic potential (associated flow), given by

$$F_{ten}(\underline{\sigma}) = Q_{ten}(\underline{\sigma}) := \sigma_{ten} - \sigma_{\min}, \Phi(F_{ten}) = F_{ten} \tag{5.16}$$

where σ_{ten} is a prescribed small tensile strength (negative value) and the fluidity parameter γ_{ten} is the same as for the plastic yield rules γ_j.

§6. 3D Shape and mapping functions

Five types of 3D elements and a doubly infinite 2D element are designed in the 3D version of **FESTER.** They are the 8-noded linear brick element, the 20-noded quadratic brick element, the 12-noded quadratic infinite brick element (*Type a*), the 7-noded quadratic doubly infinite brick element (*Type b*), the 4-noded quadratic infinite corner brick element (*Type* c) and the 3-noded quadratic doubly infinite 2D element.

6.1. Shape functions of 3D finite elements

The shape functions, with local coordinates $(s,t,\upsilon) \in [-1,1]^3$ and the numbering of the nodes shown in Figure 6.1, for the 8-noded isoparametric brick elements (tri-linear) are as follows:

$$\begin{aligned}
\phi_1(s,t,\upsilon) &= \tfrac{1}{8}\left(1-s-t+\upsilon+st+t\upsilon+st\upsilon\right),\\
\phi_2(s,t,\upsilon) &= \tfrac{1}{8}\left(1+s-t+\upsilon-st+t\upsilon-st\upsilon\right),\\
\phi_3(s,t,\upsilon) &= \tfrac{1}{8}\left(1+s+t+\upsilon+st-t\upsilon+st\upsilon\right),\\
\phi_4(s,t,\upsilon) &= \tfrac{1}{8}\left(1-s+t+\upsilon-st-t\upsilon-st\upsilon\right),\\
\phi_5(s,t,\upsilon) &= \tfrac{1}{8}\left(1-s-t-\upsilon+st+t\upsilon-st\upsilon\right),\\
\phi_6(s,t,\upsilon) &= \tfrac{1}{8}\left(1+s-t-\upsilon-st+t\upsilon+st\upsilon\right),\\
\phi_7(s,t,\upsilon) &= \tfrac{1}{8}\left(1+s+t-\upsilon+st-t\upsilon-st\upsilon\right),\\
\phi_8(s,t,\upsilon) &= \tfrac{1}{8}\left(1-s+t-\upsilon-st-t\upsilon+st\upsilon\right).
\end{aligned} \tag{6.1}$$

The shape functions, with local coordinates (s,t,υ) and the numbering of the nodes shown in Figure 6.2, for the 20-noded isoparametric brick elements (tri-quadratic) are as follows:

$$
\begin{aligned}
\phi_1(s,t,\upsilon) &= \tfrac{1}{8}(1-s)(1-t)(1-\upsilon)(-s-t-\upsilon-2),\\
\phi_2(s,t,\upsilon) &= \tfrac{1}{4}(1-s^2)(1-t)(1-\upsilon),\\
\phi_3(s,t,\upsilon) &= \tfrac{1}{8}(1+s)(1-t)(1-\upsilon)(+s-t-\upsilon-2),\\
\phi_4(s,t,\upsilon) &= \tfrac{1}{4}(1+s)(1-t^2)(1-\upsilon),\\
\phi_5(s,t,\upsilon) &= \tfrac{1}{8}(1+s)(1+t)(1-\upsilon)(+s+t-\upsilon-2),\\
\phi_6(s,t,\upsilon) &= \tfrac{1}{4}(1-s^2)(1+t)(1-\upsilon),\\
\phi_7(s,t,\upsilon) &= \tfrac{1}{8}(1-s)(1+t)(1-\upsilon)(-s+t-\upsilon-2),\\
\phi_8(s,t,\upsilon) &= \tfrac{1}{4}(1-s)(1-t^2)(1-\upsilon),\\
\phi_9(s,t,\upsilon) &= \tfrac{1}{4}(1-s)(1-t)(1-\upsilon^2),\\
\phi_{10}(s,t,\upsilon) &= \tfrac{1}{4}(1+s)(1-t)(1-\upsilon^2),\\
\phi_{11}(s,t,\upsilon) &= \tfrac{1}{4}(1+s)(1+t)(1-\upsilon^2),\\
\phi_{12}(s,t,\upsilon) &= \tfrac{1}{4}(1-s)(1+t)(1-\upsilon^2),\\
\phi_{13}(s,t,\upsilon) &= \tfrac{1}{8}(1-s)(1-t)(1+\upsilon)(-s-t+\upsilon-2),\\
\phi_{14}(s,t,\upsilon) &= \tfrac{1}{4}(1-s^2)(1-t)(1+\upsilon),\\
\phi_{15}(s,t,\upsilon) &= \tfrac{1}{8}(1+s)(1-t)(1+\upsilon)(+s-t+\upsilon-2),\\
\phi_{16}(s,t,\upsilon) &= \tfrac{1}{4}(1+s)(1-t^2)(1+\upsilon),\\
\phi_{17}(s,t,\upsilon) &= \tfrac{1}{8}(1+s)(1+t)(1+\upsilon)(+s+t+\upsilon-2),\\
\phi_{18}(s,t,\upsilon) &= \tfrac{1}{4}(1-s^2)(1+t)(1+\upsilon),\\
\phi_{19}(s,t,\upsilon) &= \tfrac{1}{8}(1-s)(1+t)(1+\upsilon)(-s+t+\upsilon-2),\\
\phi_{20}(s,t,\upsilon) &= \tfrac{1}{4}(1-s)(1-t^2)(1+\upsilon).
\end{aligned}
\tag{6.2}
$$

6.2. Shape and mapping functions of 2D and 3D infinite elements

Using the same notation as in §6.1, the shape functions $\{\phi_i\}$ of the 12-noded infinite brick elements, with the numbering of the nodes shown in Figure 6.3, are given by:

$$
\begin{aligned}
\phi_1(s,t,\upsilon) &= \tfrac{1}{8}(1-s)(1-t)(1-\upsilon)(-s-t-\upsilon-2),\\
\phi_2(s,t,\upsilon) &= \tfrac{1}{4}(1-s^2)(1-t)(1-\upsilon),\\
\phi_3(s,t,\upsilon) &= \tfrac{1}{8}(1+s)(1-t)(1-\upsilon)(+s-t-\upsilon-2),\\
\phi_4(s,t,\upsilon) &= \tfrac{1}{4}(1+s)(1-t^2)(1-\upsilon),\\
\phi_5(s,t,\upsilon) &= \tfrac{1}{8}(1+s)(1+t)(1-\upsilon)(+s+t-\upsilon-2),\\
\phi_6(s,t,\upsilon) &= \tfrac{1}{4}(1-s^2)(1+t)(1-\upsilon),\\
\phi_7(s,t,\upsilon) &= \tfrac{1}{8}(1-s)(1+t)(1-\upsilon)(-s+t-\upsilon-2),\\
\phi_8(s,t,\upsilon) &= \tfrac{1}{4}(1-s)(1-t^2)(1-\upsilon),\\
\phi_9(s,t,\upsilon) &= \tfrac{1}{4}(1-s)(1-t)(1-\upsilon^2),\\
\phi_{10}(s,t,\upsilon) &= \tfrac{1}{4}(1+s)(1-t)(1-\upsilon^2),\\
\phi_{11}(s,t,\upsilon) &= \tfrac{1}{4}(1+s)(1+t)(1-\upsilon^2),\\
\phi_{12}(s,t,\upsilon) &= \tfrac{1}{4}(1-s)(1+t)(1-\upsilon^2),
\end{aligned}
\tag{6.3}
$$

and the corresponding mapping functions $\{\psi_i\}$ are given by:

$$
\begin{aligned}
\psi_1(s,t,\upsilon) &= \tfrac{1}{2}(1-s)(1-t)(-s-t-\upsilon-2)/(1-\upsilon),\\
\psi_2(s,t,\upsilon) &= (1-s^2)(1-t)/(1-\upsilon),\\
\psi_3(s,t,\upsilon) &= \tfrac{1}{2}(1+s)(1-t)(+s-t-\upsilon-2)/(1-\upsilon),\\
\psi_4(s,t,\upsilon) &= \tfrac{1}{2}(1+s)(1-t^2)/(1-\upsilon),\\
\psi_5(s,t,\upsilon) &= \tfrac{1}{2}(1+s)(1+t)(+s+t-\upsilon-2)/(1-\upsilon),\\
\psi_6(s,t,\upsilon) &= \tfrac{1}{2}(1-s^2)(1+t)/(1-\upsilon),\\
\psi_7(s,t,\upsilon) &= \tfrac{1}{2}(1-s)(1+t)(-s+t-\upsilon-2)/(1-\upsilon),\\
\psi_8(s,t,\upsilon) &= \tfrac{1}{2}(1-s)(1-t^2)/(1-\upsilon),\\
\psi_9(s,t,\upsilon) &= \tfrac{1}{4}(1-s)(1-t)(1+\upsilon)/(1-\upsilon),\\
\psi_{10}(s,t,\upsilon) &= \tfrac{1}{4}(1+s)(1-t)(1+\upsilon)/(1-\upsilon),\\
\psi_{11}(s,t,\upsilon) &= \tfrac{1}{4}(1+s)(1+t)(1+\upsilon)/(1-\upsilon),\\
\psi_{12}(s,t,\upsilon) &= \tfrac{1}{4}(1-s)(1+t)(1+\upsilon)/(1-\upsilon),
\end{aligned}
\tag{6.4}
$$

The shape functions $\{\phi_i\}$ of the 7-noded infinite brick elements *(Type a)*,with the numbering of the nodes shown in Figure 6.4, are given by:

$$
\begin{aligned}
\phi_1(s,t,v) &= \tfrac{1}{8}(1-s)(1-t)(1-v)(-s-t-v-2),\\
\phi_2(s,t,v) &= \tfrac{1}{4}(1-s^2)(1-t)(1-v),\\
\phi_3(s,t,v) &= \tfrac{1}{8}(1+s)(1-t)(1-v)(+s-t-v-2),\\
\phi_4(s,t,v) &= \tfrac{1}{4}(1+s)(1-t^2)(1-v),\\
\phi_5(s,t,v) &= \tfrac{1}{4}(1-s)(1-t^2)(1-v),\\
\phi_6(s,t,v) &= \tfrac{1}{4}(1-s)(1-t)(1-v^2),\\
\phi_7(s,t,v) &= \tfrac{1}{4}(1+s)(1-t)(1-v^2),
\end{aligned}
\tag{6.5}
$$

and the corresponding mapping functions $\{\psi_i\}$ are given by:

$$
\begin{aligned}
\psi_1(s,t,v) &= \tfrac{1}{2}(1-s)(tv-4s-3t-3v-7)/(1-t)(1-v),\\
\psi_2(s,t,v) &= 4(1-s^2)/(1-t)(1-v),\\
\psi_3(s,t,v) &= \tfrac{1}{2}(1+s)(tv+4s-3t-3v-7)/(1-t)(1-v),\\
\psi_4(s,t,v) &= (1+s)(1+t)/(1-t)(1-v),\\
\psi_5(s,t,v) &= (1-s)(1+t)/(1-t)(1-v),\\
\psi_6(s,t,v) &= (1-s)(1+v)/(1-t)(1-v),\\
\psi_7(s,t,v) &= (1+s)(1+v)/(1-t)(1-v).
\end{aligned}
\tag{6.6}
$$

The shape functions $\{\psi_i\}$ of the 4-noded infinite brick elements *(Type* 6), with the numbering of the nodes shown in Figure 6.5, are given by:

$$
\begin{aligned}
\phi_1(s,t,v) &= \tfrac{1}{8}(1-s)(1-t(1-v)(-s-t-v-2),\\
\phi_2(s,t,v) &= \tfrac{1}{4}(1-s^2)(1-t)(1-v),\\
\phi_3(s,t,v) &= \tfrac{1}{4}(1-s)(1-t^2)(1-v),\\
\phi_4(s,t,v) &= \tfrac{1}{4}(1-s)(1-t)(1-v^2),
\end{aligned}
\tag{6.7}
$$

and the corresponding mapping functions $\{\psi_i\}$ are given by:

$$
\begin{aligned}
\psi_1(s,t,v) &= \left[(-stv+st+sv+tv+5(-s-t-v)-11\right]/(1-s)(1-t)(1-v),\\
\psi_2(s,t,v) &= 4(1+s)/(1-s)(1-t)(1-v),\\
\psi_3(s,t,v) &= 4(1+t/(1-s)(1-t)(1-v),\\
\psi_4(s,t,v) &= 4(1+v)/(1-s)(1-t)(1-v).
\end{aligned}
\tag{6.8}
$$

The shape functions $\{\phi_i\}$ of the 3-noded doubly infinite elements (2D) with the numbering of the nodes shown in Figure 6.6, are given by:

$$\begin{aligned}
\phi_1(s,t) &= \tfrac{1}{4}(1-s)(1-t)(-1-s-t),\\
\phi_2(s,t) &= \tfrac{1}{2}(1-s^2)(1-t),\\
\phi_3(s,t) &= \tfrac{1}{2}(1-s)(1-t^2),
\end{aligned} \tag{6.9}$$

and the corresponding mapping functions $\{\psi_i\}$ given by:

$$\begin{aligned}
\psi_1(s,t) &= [st+3(-1-s-t)]/(1-s)(1-t),\\
\psi_2(s,t) &= 2(1+s)/(1-s)(1-t),\\
\psi_3(s,t) &= 2(1+t)/(1-s)(1-t),
\end{aligned} \tag{6.10}$$

For completeness, we also give the shape and mapping functions of the 2D 5-noded singly infinite elements which are also used in **FESTER** (cf. [34]). The numbering of nodes of this element is shown in Figure 6.7.

$$\begin{aligned}
\phi_1(s,t) &= \tfrac{1}{4}(1-s)(1-t)(-1-s-t),\\
\phi_2(s,t) &= \tfrac{1}{2}(1-s^2)(1-t),\\
\phi_3(s,t) &= \tfrac{1}{4}(1+s)(1-t)(-1+s-t),\\
\phi_4(s,t) &= \tfrac{1}{2}(1+s)(1-t^2),\\
\phi_5(s,t) &= \tfrac{1}{2}(1-s)(1-t^2),
\end{aligned} \tag{6.11}$$

The corresponding mapping functions $\{\psi_i\}$ are given by:

$$\begin{aligned}
\psi_1(s,t) &= (1-s)(-1-s-t)/(1-t),\\
\psi_2(s,t) &= 2(1-s^2)/(1-t),\\
\psi_3(s,t) &= (1+s)(-1+s-t)/(-1+s)(1-t),\\
\psi_4(s,t) &= \tfrac{1}{2}(1+s)(1+t)/(1-t),\\
\psi_5(s,t) &= \tfrac{1}{2}(1-s)(1+t)/(1-t),
\end{aligned} \tag{6.12}$$

Remark 6.1. It can be seen clearly that the mapping functions $\{\psi_i\}$ for any of the above infinite elements do not form a partition of unity. That is

$$\sum_i \psi_i(s,t,\upsilon) \neq 1, \quad \forall (s,t,\upsilon) \in \mathbf{R}^3. \tag{6.13}$$

This means that these mapping functions are dependent of the choice of the coordinate system, i. e., they are not coordinate-free. This is because our assumption that at infinity the displacements are zero.

Remark 6.2. Other infinite 1D/2D/3D elements which extend to infinity in one/two/three direction(s) (cf. [19]) may also be introduced into **FESTER** similarly.

Remark 6.3. In the description of 2D elements, the notation for the local coordinate system used in [34] is (ξ,η), which is different from our notation (s,t).

Remark 6.4. The order of nodes in an element must be consistent with the order showing on the standard elements in the Figures 6.1-6.7. Otherwise, negative Jacobian determinants may occur which may cause incorrect results.

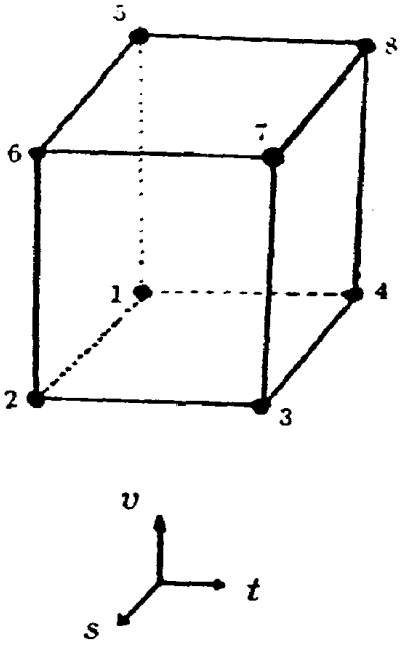

Figure 6.1

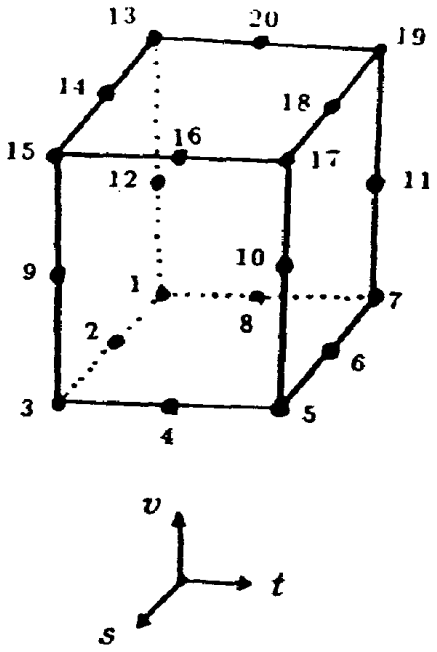

Figure 6.2

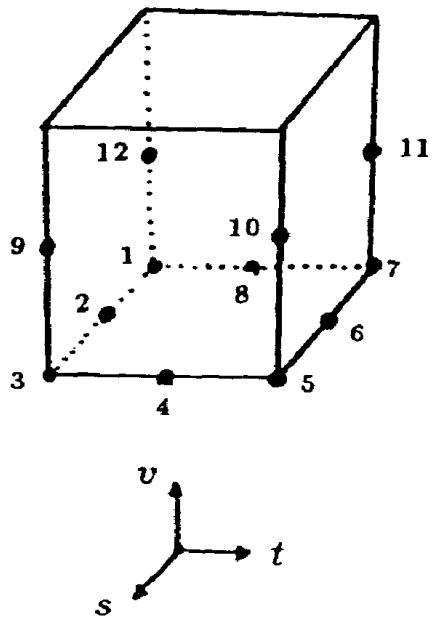

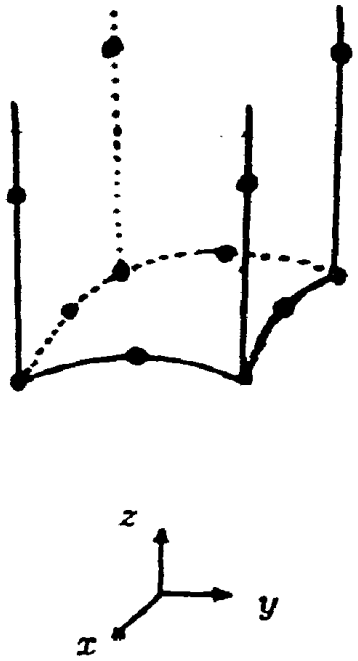

Figure 6.3

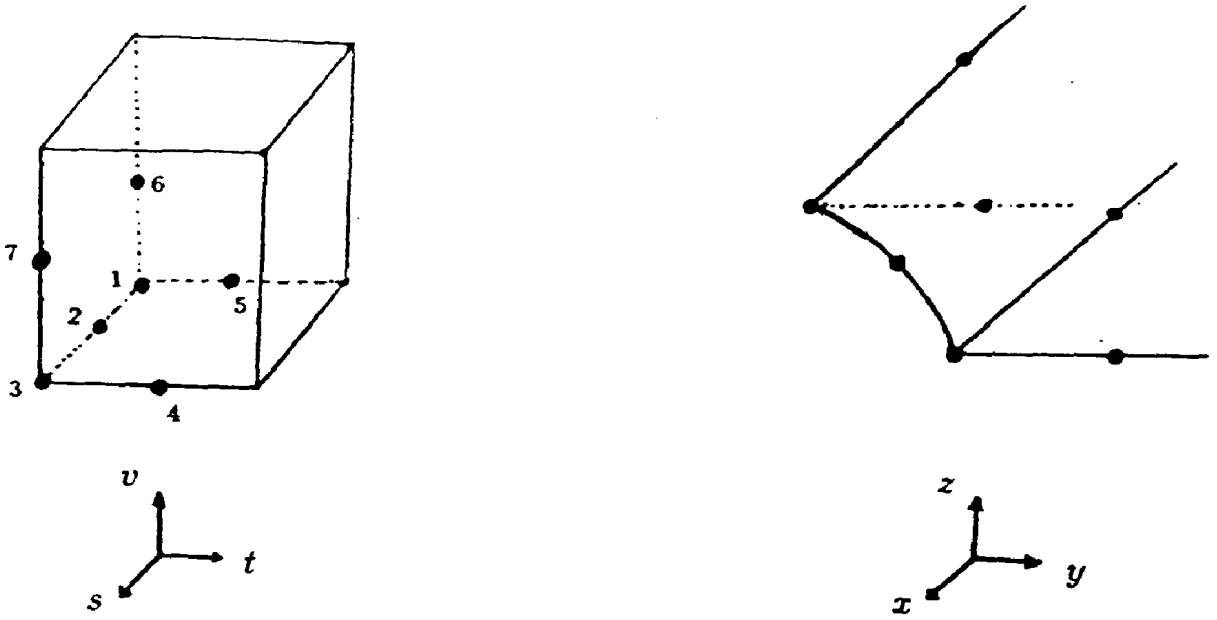

Figure 6.4

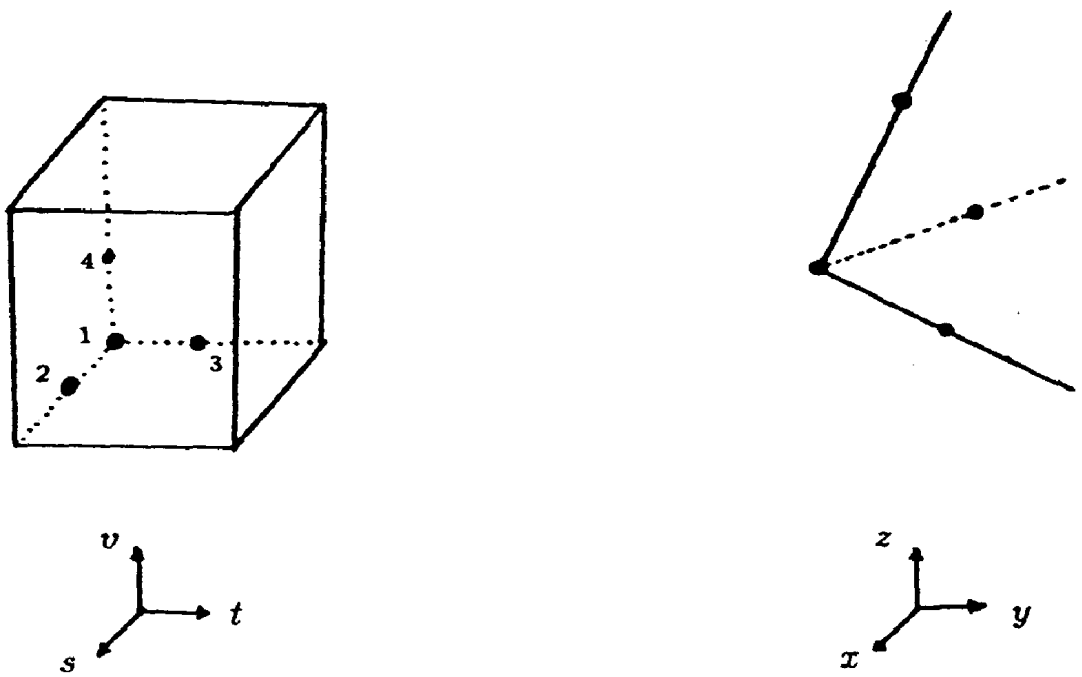

Figure 6.5

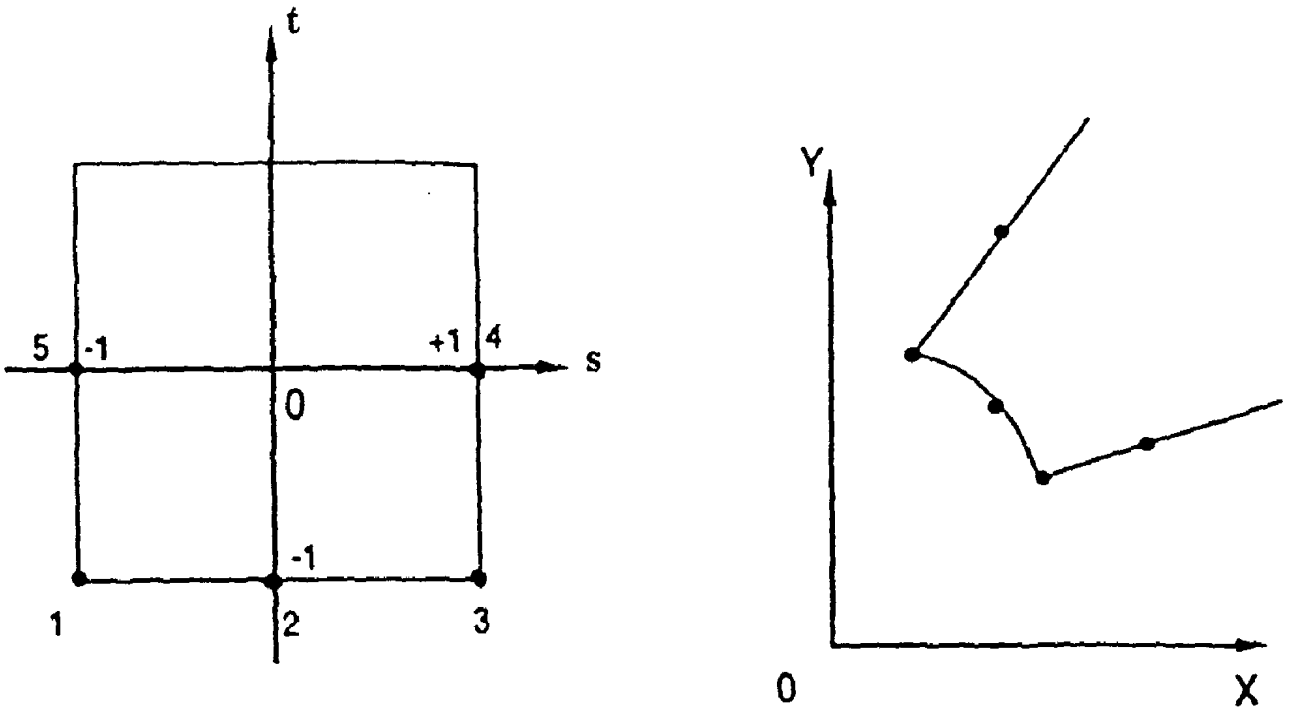

Figure 6.6

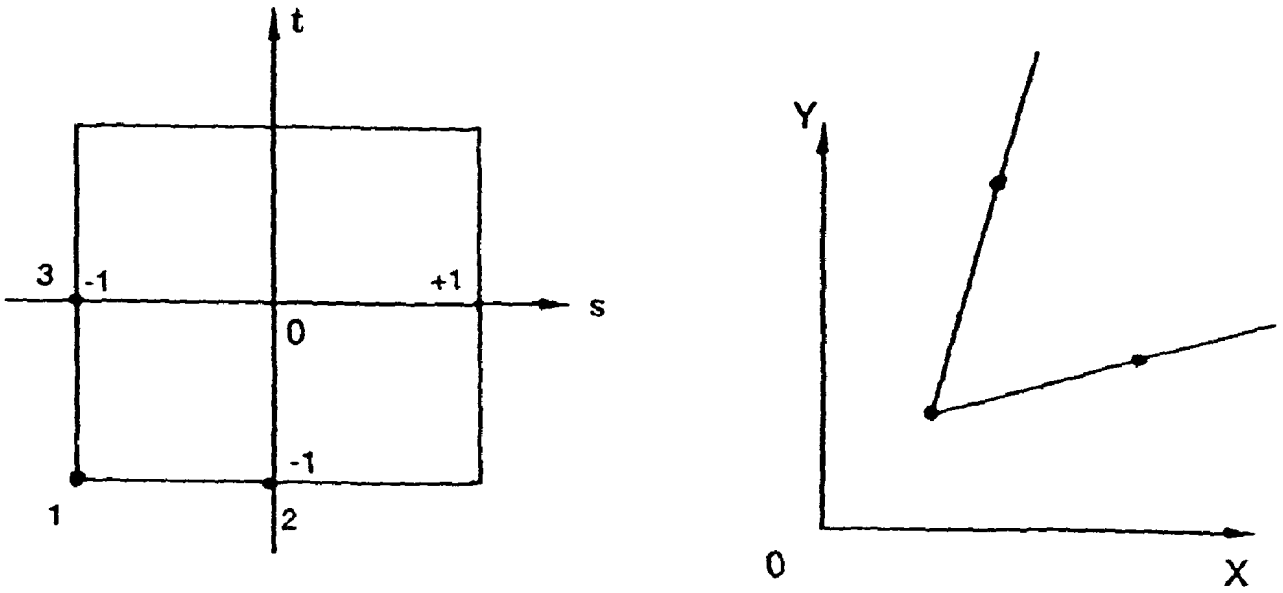

Figure 6.7

§7. Large deformation analysis and its B—matrix

In this section, we present a formulation of the large deformation analyses in the 3D version **FESTER** and the derivation of its B-matrix.

7.1. Large deformation formulation

The program is designed not only for small deformation analyses, but also for large deformation analyses. For the large deformation problems (option **NLAPS=2** in the program), the second order terms, which are non-linear terms, are also considered in the strain-displacement relations in order to obtain better approximations. That is, in this case, the strain-displacement relation is defined explicitly by [1,8,11,26]:

$$\{\in\} = \begin{Bmatrix} \in \\ \in_y \\ \in_z \\ \gamma_{xy} \\ \gamma_{xz} \\ \gamma_{yz} \end{Bmatrix} = \begin{bmatrix} \frac{\partial u_n}{\partial x} + \frac{1}{2}\left(\frac{\partial u_n}{\partial x}\right)^2 + \frac{1}{2}\left(\frac{\partial v_n}{\partial x}\right)^2 + \frac{1}{2}\left(\frac{\partial w_n}{\partial x}\right)^2 \\ \frac{\partial v_n}{\partial y} + \frac{1}{2}\left(\frac{\partial u_n}{\partial y}\right)^2 + \frac{1}{2}\left(\frac{\partial v_n}{\partial y}\right)^2 + \frac{1}{2}\left(\frac{\partial w_n}{\partial y}\right)^2 \\ \frac{\partial w_n}{\partial z} + \frac{1}{2}\left(\frac{\partial u_n}{\partial z}\right)^2 + \frac{1}{2}\left(\frac{\partial v_n}{\partial z}\right)^2 + \frac{1}{2}\left(\frac{\partial w_n}{\partial z}\right)^2 \\ \frac{\partial u_n}{\partial y} + \frac{\partial v_n}{\partial x} + \frac{\partial u_n}{\partial x}\frac{\partial u_n}{\partial y} + \frac{\partial v_n}{\partial x}\frac{\partial v_n}{\partial y} + \frac{\partial w_n}{\partial x}\frac{\partial w_n}{\partial y} \\ \frac{\partial u_n}{\partial z} + \frac{\partial w_n}{\partial x} + \frac{\partial u_n}{\partial x}\frac{\partial u_n}{\partial z} + \frac{\partial v_n}{\partial x}\frac{\partial v_n}{\partial z} + \frac{\partial w_n}{\partial x}\frac{\partial w_n}{\partial z} \\ \frac{\partial w_n}{\partial y} + \frac{\partial v_n}{\partial z} + \frac{\partial u_n}{\partial z}\frac{\partial u_n}{\partial y} + \frac{\partial v_n}{\partial z}\frac{\partial v_n}{\partial y} + \frac{\partial w_n}{\partial z}\frac{\partial w_n}{\partial y} \end{bmatrix} \tag{7.1}$$

where $\in_x, \in_y, \in_z, \gamma_{xy}, \gamma_{xz}, \gamma_{yz}$ are the strain components and u_n, v_n, w_n are the displace- ments at the time step t_n (an incremental loading procedure is used in **FESTER** for nonlinear problems).

Since the nonlinear terms are introduced, the (element) stiffness matrix, **K**, is thus composed of two parts, $\mathbf{K}_{lin}$, and $\mathbf{K}_{non}$, *i. e.*, $\mathbf{K} = \mathbf{K}_{lin} + \mathbf{K}_{non}$, Here, $\mathbf{K}_{lin}$ is the contribution from the linear part and K_{non} is that from the nonlinear part. In **FESTER,** special subroutines, BMAT, MOD2, EMAT and GMAT, are designed to compute $\mathbf{K}_{lin}$ and $\mathbf{K}_{non}$ separately and then sum them up to obtain the total (nonlinear) stiffness matrix **K**.

7.2. B-matrix formulation

To form the stiffness matrix for 3D stress-strain analyses, we first need to formulate the strain-displacement relations, *i.e.,* the B-matrix. Suppose the shape functions are denoted by ϕ_i, i=l,2,...,n and the nodal displacements by $\mathbf{d}_i°, i = 1,2, \ldots, n$, then the displacement **d** at point (x, y, z) in the global coordinates syste ((ξ, η, ζ) in the local

coordinates system) is given by

$$\mathrm{d} = \sum_{i=1}^{n} \mathrm{d}_i^0 \, \phi_i . \tag{7.2}$$

The strains at this point are given by a similar formula to (7.1).

For small deformations, we can obtain, by suitable substitutions and arrangements:

$$\underline{\in}_{lin} = \sum_{i=1}^{n} \mathrm{B}_{lin,i} \, \mathrm{d}_i^0 \tag{7.3}$$

where $\mathrm{B}_{lin,i}$ is the linear part of the i-th strain matrix, which is given by

$$\mathrm{B}_{lin,i} := \begin{pmatrix} \frac{\partial \phi_i}{\partial x} & 0 & 0 \\ 0 & \frac{\partial \phi_i}{\partial y} & 0 \\ 0 & 0 & \frac{\partial \phi_i}{\partial x} \\ \frac{\partial \phi_i}{\partial y} & \frac{\partial \phi_i}{\partial x} & 0 \\ \frac{\partial \phi_i}{\partial z} & 0 & \frac{\partial \phi_i}{\partial x} \\ 0 & \frac{\partial \phi_i}{\partial z} & \frac{\partial \phi_i}{\partial y} \end{pmatrix} \tag{7.4}$$

By defining:

$$\mathrm{B}_{lin} := (\mathrm{B}_{lin,1}, \mathrm{B}_{lin,2}, ..., \mathrm{B}_{lin,n}), \tag{7.5}$$

$$\mathrm{d}^0 := (\mathrm{d}_1^0, \mathrm{d}_2^0, ..., \mathrm{d}_n^0)^t ,$$

we have

$$\underline{\varepsilon}_{lin} = \mathrm{B}_{lin} \, \mathrm{d}^0 . \tag{7.6}$$

Hence the global stiffness matrix (linear part) K_{lin} and the element stiffness matrix $\mathrm{K}_{lin,i,j}$, $i,j = 1,2, \ldots,n$ are given by

$$\begin{cases} \mathrm{K}_{lin,i,j} & = \mathrm{B}_{lin,i}^t \mathrm{D} \mathrm{B}_{lin,j} , \\ \mathrm{K}_{lin} & = \mathrm{B}_{lin}^t \mathrm{D} \mathrm{B}_{lin} = (\mathrm{K}_{lin,i,j}), \end{cases} \tag{7.7}$$

where D is the strain-stress matrix (constitutive law (5.1)).

For large deformations, the formulation is the similar but the nonlinear terms in (7.1) are also considered in the formulation of .the strain matrices, that is, $\mathrm{B}_i = \mathrm{B}_{lin,I} + \mathrm{B}_{non,i}$, $i = 1,2, \ldots,n$, where $\mathrm{B}_{lin,i}$ is given by (7.4) and $\mathrm{B}_{non,i}$ is the non-linear part of the strain matrix. More explicitly, for $i = 1,2, \ldots,n$, $\mathrm{B}_{non,i}$ is given by

$$\mathbf{B}_{non,i} := \begin{pmatrix} \frac{1}{2}\frac{\partial \phi_i}{\partial x}\sum_{j=1}^{n} u_j \frac{\partial \phi_j}{\partial x} & \frac{1}{2}\frac{\partial \phi_i}{\partial x}\sum_{j=1}^{n} v_j \frac{\partial \phi_j}{\partial x} & \frac{1}{2}\frac{\partial \phi_i}{\partial x}\sum_{j=1}^{n} w_j \frac{\partial \phi_j}{\partial x} \\ \frac{1}{2}\frac{\partial \phi_i}{\partial y}\sum_{j=1}^{n} u_j \frac{\partial \phi_j}{\partial y} & \frac{1}{2}\frac{\partial \phi_i}{\partial y}\sum_{j=1}^{n} v_j \frac{\partial \phi_j}{\partial y} & \frac{1}{2}\frac{\partial \phi_i}{\partial y}\sum_{i=1}^{n} w_j \frac{\partial \phi_j}{\partial y} \\ \frac{1}{2}\frac{\partial \phi_i}{\partial z}\sum_{j=1}^{n} u_j \frac{\partial \phi_j}{\partial z} & \frac{1}{2}\frac{\partial \phi_i}{\partial z}\sum_{j=1}^{n} v_j \frac{\partial \phi_j}{\partial z} & \frac{1}{2}\frac{\partial \phi_i}{\partial z}\sum_{j=1}^{n} w_j \frac{\partial \phi_j}{\partial z} \\ \frac{\partial \phi_i}{\partial x}\sum_{j=1}^{n} u_j \frac{\partial \phi_j}{\partial y} & \frac{\partial \phi_i}{\partial x}\sum_{j=1}^{n} v_j \frac{\partial \phi_j}{\partial y} & \frac{\partial \phi_i}{\partial x}\sum_{j=1}^{n} w_j \frac{\partial \phi_j}{\partial y} \\ \frac{\partial \phi_i}{\partial x}\sum_{j=1}^{n} u_j \frac{\partial \phi_j}{\partial z} & \frac{\partial \phi_i}{\partial x}\sum_{j=1}^{n} v_j \frac{\partial \phi_j}{\partial z} & \frac{\partial \phi_i}{\partial x}\sum_{j=1}^{n} w_j \frac{\partial \phi_j}{\partial z} \\ \frac{\partial \phi_i}{\partial y}\sum_{j=1}^{n} u_j \frac{\partial \phi_j}{\partial z} & \frac{\partial \phi_i}{\partial y}\sum_{j=1}^{n} v_j \frac{\partial \phi_i}{\partial z} & \frac{\partial \phi_i}{\partial y}\sum_{j=1}^{n} w_j \frac{\partial \phi_i}{\partial z} \end{pmatrix} \tag{7.8}$$

Hence, the i-th total strain matrix, $\mathbf{B}_i$ which is composed of the linear part $\mathbf{B}_{lin,i}$ and the non-linear part $\mathbf{B}_{non,i}$, is given by:

$$\mathbf{B}_i := \mathbf{B}_{lin,i} + \mathbf{B}_{non,i} \qquad i = 1,2,..., n. \tag{7.9}$$

Similar to the formulation of linear strain-displacement relation, we have:

$$\mathbf{B}:=(\mathbf{B}_1,\mathbf{B}_2,...,\mathbf{B}_n), \tag{7.10}$$

and

$$\underline{\varepsilon} = \mathbf{B}\mathbf{d}^0. \tag{7.11}$$

Hence the total global stiffness matrix $\mathbf{K}$ and the element stiffness matrix $\mathbf{K}_{i,j}, i,j$ = 1,2, …,n are given by

$$\begin{cases} \mathbf{K}_{i,j} & = \mathbf{B}_i^t \mathbf{D}\mathbf{B}_j, \\ \mathbf{K} & = \mathbf{B}^t \mathbf{D}\mathbf{B} = (\mathbf{K}_{i,j}), \end{cases} \tag{7.12}$$

Since the matrices $\mathbf{B}_{non,i}$, $i = 1,2, \ldots,n$, depend on the displacement $\mathbf{d}°$, (7.11) is not a linear relation. In fact, from (7.8), it is obvious that $\underline{\varepsilon}$ is a quadratic function of $\mathbf{d}°$.

§8. Other modifications to FESTER

In this part, we state some differences between the 3D version program of **FESTER** and its 2D version.

8.1. Modifications to subroutines

In addition to many minor changes to almost all the subroutines in the 2D version program to adapt it for 3D analyses, big changes were made to the following subroutines: TMAT, BMAT, INVAR, JNTB, MOD2, MODJ.

A. *Modifications to* **INVAR**

The subroutine INVAR can be used to compute the following values; their mathematical formulations are given in §3:

a. Stress/strain Invariants $I_1, I_2, I_3, J_2, J_3, \theta$;

b. The first derivatives of these invariants;

c. The second derivatives of these invariants;

d. The first/second derivatives of the principal stresses;

e. The b and a vectors for the HB/DP flow rules and the tensile cracking rule.

B. *Modifications to* **BMAT**

The subroutine BMAT generates the linear part of the the B-matrix, B_{lin}, for both small and large deformation analyses in 3D problems.

C. *Modifications to* **JNTB**

The subroutine JNTB produces the joint element B-matrix B_{jnt} for both 1D and 2D joint elements. In the 2D case, it is restricted to the 16-noded quadratic element only.

D. *Modifications to* **MMAT** *and* **GMAT**

Subroutines MMAT and GMAT produce the non-linear part of the the B-matrix, B_{non}, for both 2D and 3D large deformation analyses. That is, the strain matrix B is given by $B_{lin} + B_{non}$ (cf. §7).

E. *Modifications to* **MODJ**

The subroutine MODJ produces the *D-matrix* for 1D and 2D joint elements.

F. *Modifications to* **MOD2**

The subroutine MOD2 produces the *D-matrix* for 2D and 3D orthotropic materials. In the 3D case, the orientation of the orthotropic material should be provided by three unit vectors: (v_1, v_2, v_3) in the reference coordinate system, with the plane of weakness in the plane spanned by v_1 and v_2.

G. *Modifications to* **SFR**

The subroutine SFR produces the shape functions of the 12 types of 2D and 3D elements which are described in §2.2.3. The subroutine MAPFUN are modified similarly to generate the three mapping functions of the 2D and 3D infinite elements.

8.2. Other modifications

There are some other changes to the 2D version program. The following list may be helpful to understand the difference between the two versions.

A. *Input and output formats*

Since the brick elements are used in the 3D version, all formats concerning the input and output of the elements, stress and strain vectors, loading, displacements etc. are rewritten. The formats in the new version can also be used to analyse 2D and axial symmetric problems with the same input and output formats as in the 2D version. For 3D problems, the stress output (at Gaussian points) is quite different from that produced by its 2D version. The stress outputs include: principal stresses σ_1, σ_2, σ_3 their directions (principal directions) in $\mathbf{R}^3$: α_1, α_2, α_3 and the yield indicator, which is the same as in the 2D version. The displacement output differs only a little: the displacements are vectors in $\mathbf{R}^3$ instead of in $\mathbf{R}^2$.

B. *Common block*

A Common Block is designed in the 3D version program. The block is composed of some constants which are frequently used in the program. The element type array, LTYPE, is also stored in this block.

C. *New subroutines*

Two subroutines are added to the program: **MULTAB** and **CROSS.** The subroutine **MULTAB** multiplies two matrices and **CROSS** is used to find the Cross-Product of two vectors.

D. *Gauss quadrature rule*

In order to increase the accuracy of computer results for 3D stress-strain analyses, the order of the Gaussian quadrature which is used to obtain the stiffness matrix and the nodal forces, is set to 3 even if the input value NGAUS ≠ 3. In this way, some near-singular cases can also be calculated by the program. Otherwise, there may be near-zero pivot values. However, for the 3D 8-noded, 20-noded and infinite elements the default number of Gaussian points of each element at which the stresses and displacements are to be computed and output is 8.

§9. Numerical examples

Four numerical examples are given in this section to demonstrate some of the mathematical models employed in the 3D version of **FESTER.** They are the Large Displacement, 3D Infinite Element and 2D Joint Element models. Two examples are also given to show the program being used for solving practical problems.

Example 9.1. Large Displacement: 3D Cantilever Analyses. The results are shown in Figures 9.1-9.4.

Example 9.2. Joint Element: Sliding between two Rock Strata. The results are shown in Figures 9.5-9.8.

Example 9.3. A 3D stress distribution in a rock stratum. The results are shown in Figures 9.9-9.10.

§10. Conclusions

In this report, a detailed description of the nonlinear finite element program **FESTER** for 3D analyses is presented. The package is specially designed for deep-level tunnel excavation analyses. The theory used to model the (3D) rock behaviour and numerical method used in the 3D program are the same as for the 2D analyses. However, many changes have been made to suit 3D applications. The main features of the 3D analyses are as follows:

1. The mapped 3D infinite elements are used to simulate the far field deformation;

2. The 2D joint elements (surface contact) are used to model the sliding (discontinuous displacements, stresses and strains) behaviour between two rock strata and in the joints in rock masses;

3. Special treatments are given (yield criterion, plastic potential, sliding and cracking rule) to the plane of weakness in 3D for orthotropic materials (rocks);

4. 3D large displacement problems can also be analysed (the second order terms in the strain-displacement relations have been taken into account in the program);

5. A variety of (3D) yield criteria and plastic potentials (Mohr-Coulomb, Hoek—Brown and Drucker-Prager) for both associated and non-associated flow rules are employed;

6. Different techniques to simulate the tunnel excavation process are used in the program: incremental loading, stress and stiffness reduction and any combination of these two processes.

References

1. Bathe, K. J., **Finite Element Procedures in Engineering Analysis,** Englewood cliffs: Prentice-Hall Inc., 1982.
2. Beer, G., 'An isoparametric joint/interface element for finite element analysis', Int. J , for Numer. Meth. in Engg., Vol. **21**, 1985, 585-600.
3. Bieniawski, Z. T., 'Rock mass classification in rock engineering', *Exploration for Rock Engineering,* ed. Z. T. Bieniawski, Vol. **1**, Rotterdam, Balkema, 1976, 97-106.
4. Brady, B. H. G. and Brown, E. T., **Rock Mechanics for Underground Mining,** London: George Allen &; Unwin., 1985
5. Brady, B. H. G., 'Boundary element and linked methods for underground excavation design', *Introduction in Analytical and Computational Methods in Engineering Rock Mechanics,* London: Allen &: Unwin, 1987, 164-204.
6. Brown, E. T. (eds.), **Analytical and Computational Methods in Engineering Rock Mechanics,** Allen & Unwin, London, 1987.
7. Carter, J. P., Booker, J. R. and Davis E. H., 'Finite deformation of an elasto-plastic Soil', *Int. J. Num. Anal. Meth. Geomech.,* Vol.1, 1977, 25-43.
8. Chen, W. F. and Saleeb, **A. F., Constitutive Equations for Engineering Materials,** John Wiley & sons, NY, 1982.
9. Cundall, P. A., 'A computer model for rock mass behaviour using interactive graphics', U.S. Army, Corps of Engineers, Technical Report MRP2-74, Missouri River Division, 1974.
10. Cundall, P. A. and Marti, J., 'Some new developments in discrete numerical methods for dynamic modelling of joint rock masses', Rapid Excavation and Tunnelling Conference, Atlanta, Geogia, 1979.
11. Desai, C. S. and Phan, H. V. 'Three dimensional finite element analysis including material and geometrical non-linearities', Computational Methods in Nonlinear Mechanics, J. T. Oden (ed.), North-Holland Publishing Company, 1980, 205-224.
12. Goodman, R. E. *et al,* 'A model for the mechanics of joint rock', J. Soil Mech. and Found. Division, Proceedings of the American Society of Civil Engineers, **ASCE 94,** 1968, 637-659.
13. Hinton, E. and Owen **D. R. J., Finite Element Programming,** Academic Press, London, 1977.
14. Hoek, E. and Brown, E. T., 'The Hoek-Brown failure criterion—a 1988 update', *Proc. 18th Canadian Rock Mech. Sym.,* Toronto, 1988.
15. Hoek, E. and Brown, E. T., 'Empirical strength criterion for rock masses. *J. of Geotech. Eng. Division,* Vol. **106**, 1980, No. GT9, 1013-1035.
16. Kiousis, P. D., Voyiadjis, G. Z. and Tumay, M. T., 'A large strain theory for the two dimensional problems in geomechanics', *Int. J. Num. Anal. Meth. Geomech., Vol.* **10,** 1986, 17-39.
17. Lekhnitskii, S. G., **Anisotropic Plates,** translated by S. W. Tsai and T. Cheron, Gorden and Breach Science Publishers, London, 1968.

18. Lama, R. D. and Vutukuri, V. S., **Hand Book on Mechanical Properties of Rocks,** Vol. **IV,** Trans Tech Publications, Germany, 1987.

19. Marques, J. M. M. C. and Owen, D. R. J., 'Infinite elements in quasi-static materially nonlinear problems', Computers & Structures, Vol. 18, No. 4, 1984, 739-751.

20. Naylor, D. J., **Finepak (Mark 2): User Instructions and Explanatory Note,** Dept. of Civil Engeg. Rep. CR/85/76, Univ. College Swansea, 1976.

21. Owen, D. R. J. and Hinton, E., **Finite Elements in Plasticity—Theory and Practice,** Pineridge Press Ltd., Swansea, U. K., 1980.

22. Pan, X. D., **'Numerical Modelling of Rock Movements Around Mine Openings,** Ph. D thesis, University of London (Imperial College), 1988.

23. Pan, X. D. and Hudson, J. A., 'A simplified three dimensional Hoek and Brown yield criterion', *Rock Mechanics and Power Plants,* M. Romana (ed.), ISRM Sym., 1988, 95-103, Madrid, Spain.

24. Pan, X. D. and Hudson, J. A., 'Plane strain analysis in modelling of 3-D tunnel excavations', *Int. J.Rock Mech. & Min. Sci. & Geomech. Abstr.,* Vol. **25,** 1988, 331-337.

25. Pan, X. D. and Reed, M. B., 'A coupled distinct—finite element method for the large deformation analysis of rock masses', Pro. of 1st *U. S. Conference of DEM,* CSM Press, (session 6B), Golden, Colorado, 1989.

26. Pan, X. D., Hudson, J. A. and Cassie, J., 'Large deformation of weak rocks at depth — a numerical case study', Proc. ISRM conference on Rock at Great Depth, Pau, France, 1989, 613-620.

27. Pan, X. D. and Reed, M. B., 'Development progress of program FESTER', Research report, Department of Maths, and Stats., Brunel University, U. K., 1990.

28. Pande, G. N. and Sharma, K. G., 'On joint /interface elements and associated problems of numerical ill-conditioning', Int. J. of Numer. Meth. Geomech., Vol. 2,1979, 293-300.

29. Poulos, H. G. and Davis, **E. H**., **Elastic Solutions for Soil &: Rock Mechanics,** John Wiley & sons, London, 1974.

30. Reed, M. B., 'Stress and displacements around a cylindrical cavity in soft rock', IMA J. of Applie, Oxford University Press, 1986, 223-245.

31 Reed, M. B., 'Numerical solutions for the axisymmetric tunnel problem using the Hoek-Brown criterion', Numer. Models in Geomech., G. N. Pande and W. F. Vam Impe eds., M. Jackson, Redruth, 1986, 369-374.

32. Reed, M. B., 'An elasto-viscoplastic model for soft rock', Eng. Comp. 5, 65-70.

33. Reed, M. B., 'Non-associated flow rules in computational plasticity', Num. Meth. in Geomech., Innsbruck 1988, G. Swoboda ed., A. A. Balkema, Rotterdam, 481-488.

34. Reed, M, B. and Lavender, **D. P**., **'FESTER**—An elasto-viscoplastic finite element program for geotechnical applications', Technical report and user manual, Department of Math. and Stats., Brunel University, U. K., 1989.

35. Shäfer, H., 'A contribution to the solution of contact problems with the aid of bond elements', Comp. Meth. in Appl. Mech. and Engg. 6, 1975, 335-354.

36. Srivastava, R. K., Sharma, K. G. and Varadarajan, A., 'Analysis of stresses in the pillar zone of twin circular interacting tunnels', Proc. of Numerical Methods in Geomechanics, (ed. Swoboda), Insbruck, 1988, 1597-1606.

37. Wilson, A. H., 'The stability of underground workings in the soft rocks of the coal measures', *Int. J. Min. Eng.,* Vol. 1, No. 2, 1983, 91-187.

38. Yamada, Y. and Wifi, A. S., 'Large strain analysis of some geomechanics problems by the finite element methods', *Int. J. Num. Anal. Meth. Geomech.,* Vol. 1, 1977, 299-318.

39. Zienkiewicz, O. C. and Nayak, G. C., 'A general approach to problems of large deformation and plasticity using isoparametric elements', *3rd Conf. Matrix Meth. Struc. Meth.,* Wright-Patterson Air Force Base, Ohio, 1973, 881-928.

40. Zienkiewicz, O. C., **The Finite Element Method,** 3rd edition, Mcgraw-Hill Book Company (U.K.) Limited, London, 1977.

41. Zienkiewicz, O. C. and Cormeau, I. C., 'Visco—plasticity, plasticity and creep in elastic solids—a unified numerical solution approach', *Int. J. Numer. Meth. Engg.,* Vol. 8, 1974, 821-845.

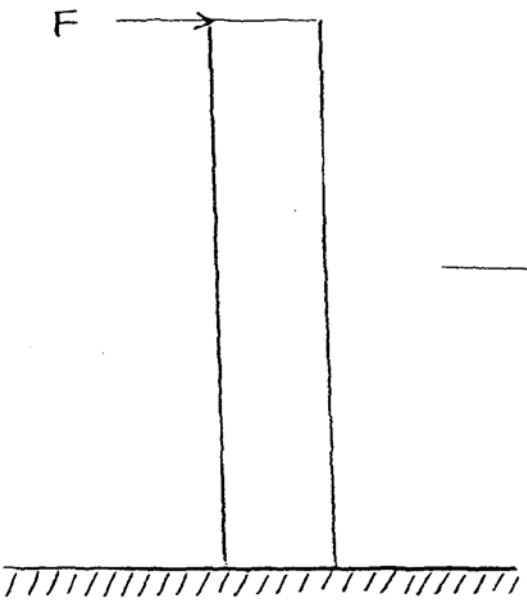

Fig. 9.1.

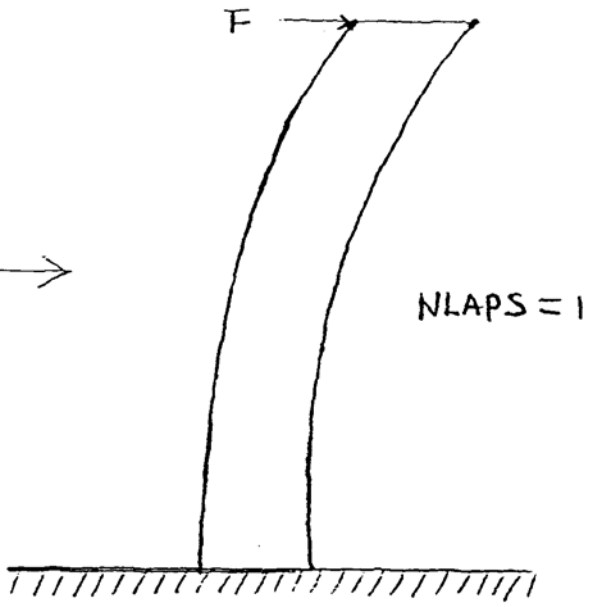

Fig. 9.2.

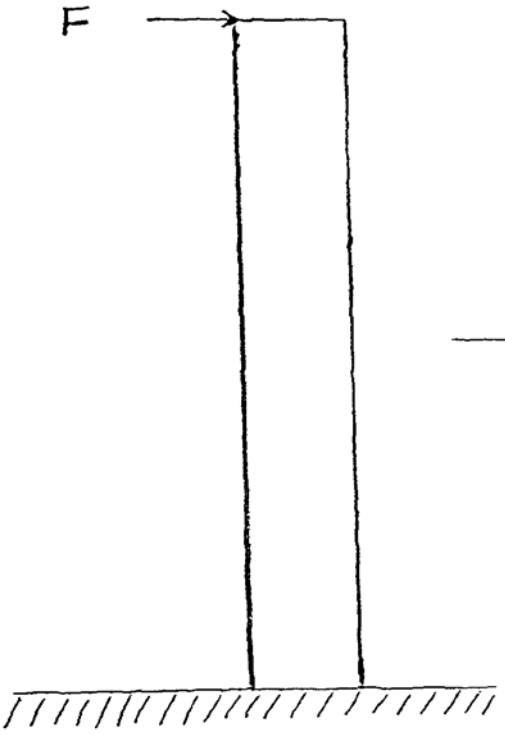

Fig. 9.3.

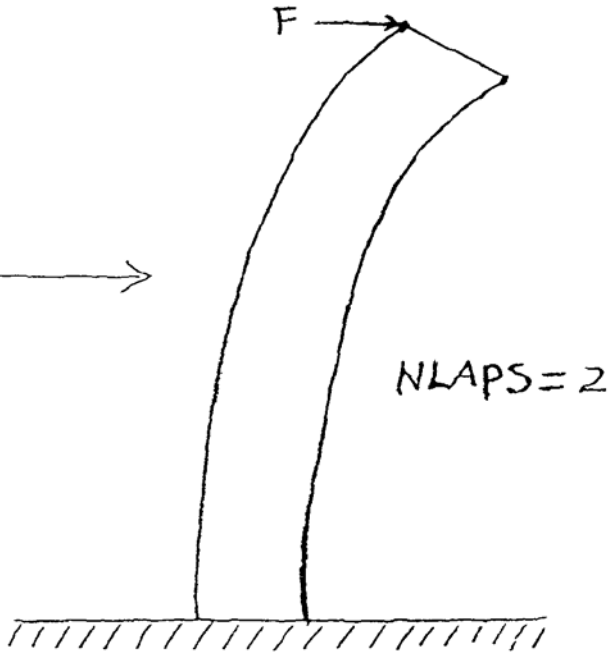

Fig. 9.4.

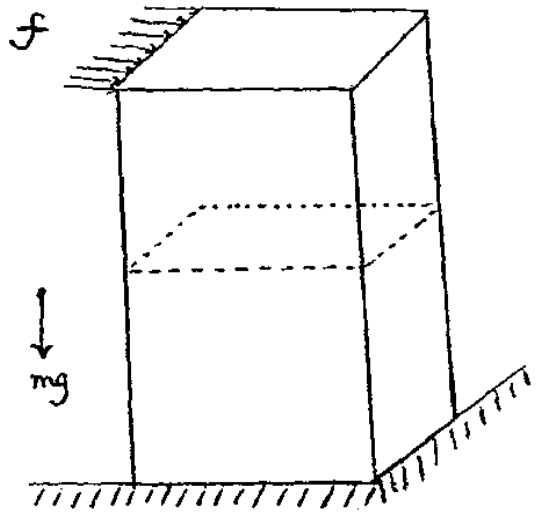

Fig. 9.5.

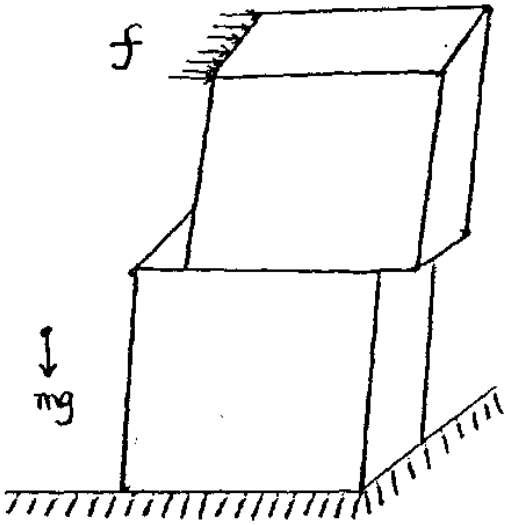

Fig. 9.6.

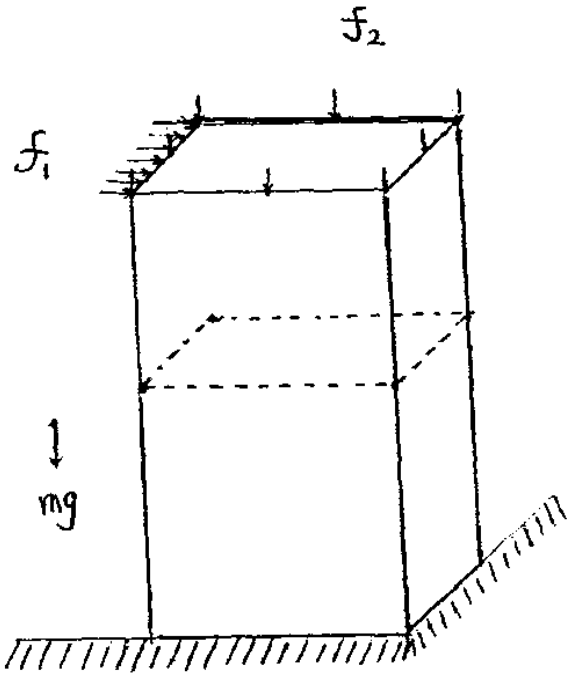

Fig. 9.7.

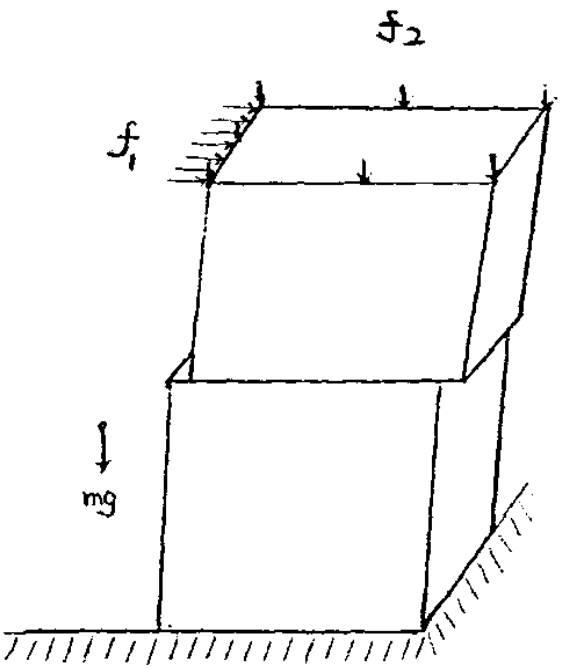

Fig. 9.8.

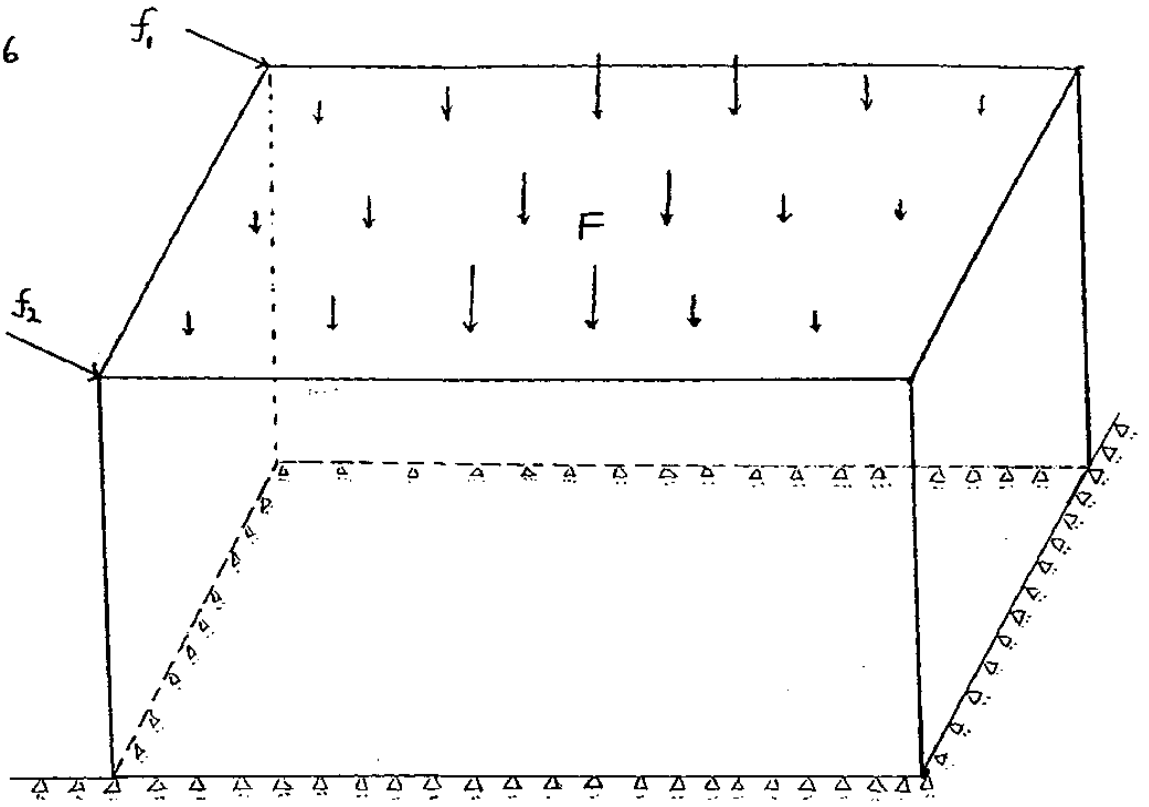

Figure 9.9.

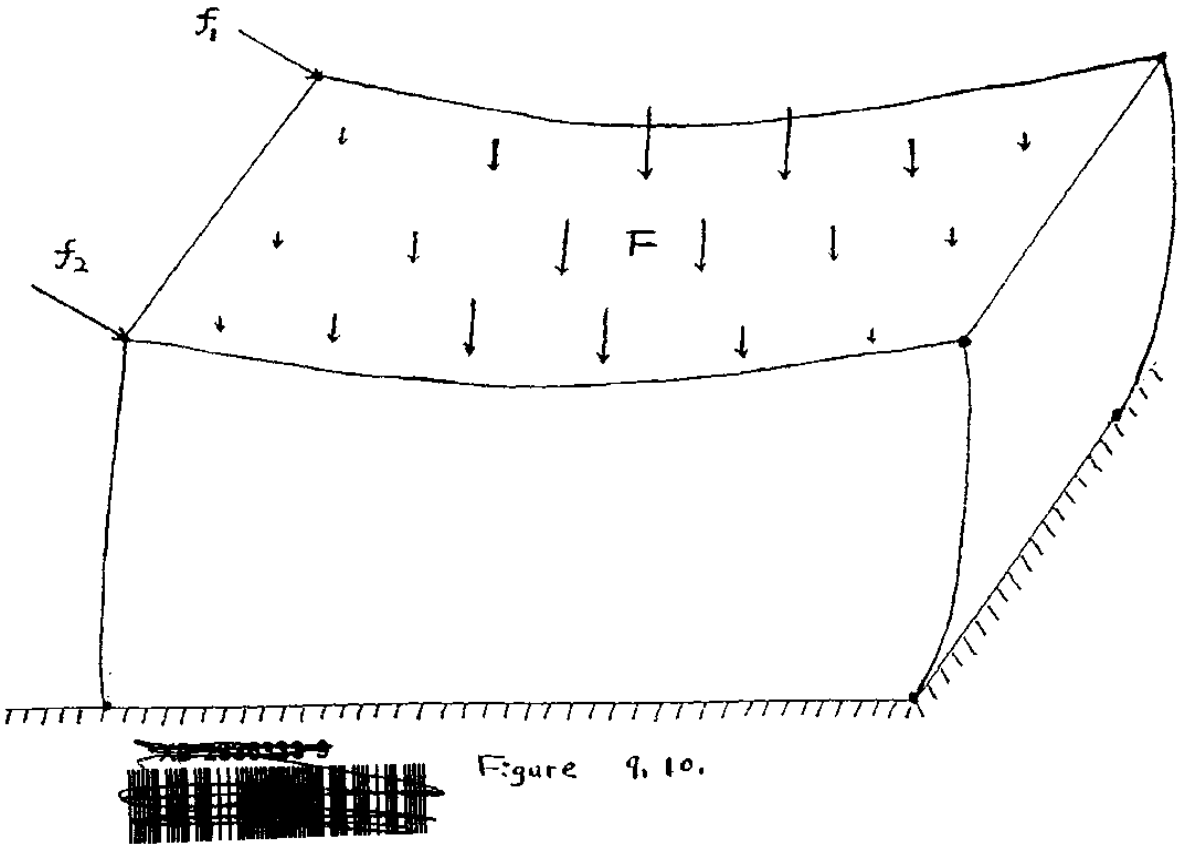

Figure 9.10.